# THERMAL ANALYSIS OF PET TARGET FOR MEDICAL CYCLOTRON

By


**SUJAAN KHAN**

**ENGG01201801052**

**Bhabha Atomic Research Centre, Mumbai**


*A thesis submitted to the*

*Board of Studies in Engineering Sciences*

*In partial fulfillment of requirements*

*for the Degree of*

**MASTER OF TECHNOLOGY**

***of***

**HOMI BHABHA NATIONAL INSTITUTE**

**December, 2020**

# HOMI BHABHA NATIONAL INSTITUTE

**Recommendations of the Thesis Examining Committee**

As members of the Thesis examining Committee, we recommend that the thesis prepared by SUJAAN KHAN entitled "THERMAL ANALYSIS OF PET TARGET FOR MEDICAL CYCLOTRON" be accepted as fulfilling the thesis requirement for the Degree of Master of Technology.

| | Name | Signature |
|---|---|---|
| Member-1 | Shri Rupul Ghosh | |
| Member-2 | Dr Pranab Bhattacharyya | |
| Technical Advisor | Dr Anjan Dutta Gupta | |
| Examiner (external) | Dr Swarnendu Sen | |
| Guide & Convener | Shri Sundeep Ghosh | |
| Chairman | Dr Paramita Mukherjee | |

Final approval and acceptance of this thesis is contingent upon the candidate's submission of the final copies of the thesis to HBNI.

I hereby certify that I have read this thesis prepared under my direction and recommend that it may be accepted as fulfilling the thesis requirement.

Date: 23/12/2020

Place: KOLKATA

Signature of the Guide

Name of the Guide: SUNDEEP GHOSH

# DECLARATION

I, hereby declare that the investigation presented in the thesis has been carried out by me. The work is original and has not been submitted earlier as a whole or in part for a degree / diploma at this or any other Institution / University.

Signature: Sujaan Khan 23/12/2020

Candidate Name: Sujaan Khan

# ACKNOWLEDGEMENTS

I would like to thank all of the members of my M.Tech monitoring committee. I would like to thank Shri. Sundeep Ghosh, my senior and guide, for all his help and guidance in completing my degree. I would like to thank Dr. Anjan Dutta Gupta, my technical advisor and mentor, for all of his faith in me and support over last seventeen months. I also owe many thanks to everyone at the Variable Energy Cyclotron Centre for their help and support.

I would like to thank my parents for everything they have done for me and all that they continue to do. I would like to thank my brother and sister for their help and encouragement.

# CONTENTS

# ABSTRACT

Radionuclide F-18, a positron emitter, is used in Positron Emission Tomography for the diagnosis of cancer cells. The emitted positron does not have a high range inside the cell and combines with the electron present in the cell leading to Annihilation of electron-positron pair producing two gamma photons. These photons are detected by the gamma detectors. F-18 is synthesized into FDG (Fluorodeoxyglucose), which acts as a radioactive tracer. Cancerous cells consume FDG at a faster rate than the normal cells. The FDG reaches more in cancerous cells and more gamma are detected from these cells spotting the malignant cells in the gamma image. One method to produce F-18 is to use proton beams on O-18 enriched water through $O^{18}(p,n)F^{18}$ reaction. As the proton beam is directed on target water, it starts producing F-18 and deposits heat due to the slowdown of the proton beam in the water medium. The yield of F-18 increases with the increase in beam current, but also large heat is generated in the water. The vaporization of water can lead to penetration of the beam through the target liquid and its interaction with the target back wall. This reduces the yield of F-18 as the beam is not interacting with the water. The purpose of this thesis work is to design a PET target chamber with adequate cooling arrangements in order to maintain a desirable void fraction of the two phase O-18 enriched water target at steady state after interaction with the incoming proton beam. This will ensure that an optimum yield of F-18 is achieved. This design will allow boiling of the liquid target where it directly interacts with the incoming proton beam. The generating bubbles will again get condensed into water when they come in contact with the relatively cold liquid around the periphery and the surface of target chamber cooled by external means. The design work is based on computational method. Transient thermal analysis was carried out to know the variation of target liquid Void Fraction with time and the results were compared with Lumped system analysis data. Structural stress analysis was done to check the stresses on Window. A 3D solid model was created based on this study.

# LIST OF FIGURES

# LIST OF TABLES

# LIST OF SYMBOLS AND ABBREVIATIONS

$\alpha$ - Void Fraction

$A$- Inside Area of pipe connected to inlet and outlet manifold ($m^2$)

$A_1$ - Area of curved surface inside target chamber

$A_2$ - Area of back inside target chamber

$A_{back}$ - Back Plate Area ($m^2$)

$A_{beam}$ - Proton Beam Area ($m^2$)

$A_r$ - Curved surface area of target chamber ($m^2$)

$A_{rad}$ - Radial channel cross-section ($m^2$)

$c_f$ - Specific heat capacity of liquid (J/Kg-K)

*CT*- Computed Tomography

$d$ - Jet exit diameter (m)

$d_r$ - Radial channel diameter (m)

$D_e$ - Exit pipe diameter (m)

$D$ - Inner diameter of pipe connected to back jet nozzle (m)

$D_{imp}$ - Jet impingement diameter (m)

$D_o$ - Outer diameter of pipe connected to back jet nozzle (m)

$\frac{\partial E}{\partial x}$ - Stopping Power in a material (MeV/mm)

$E$ - Proton Energy (MeV)

$f$ - Friction factor

*FDG* - Fluorodeoxyglucose

$g$ - Acceleration due to gravity (9.81m/s$^2$)

$h_{boil}$ - Boiling heat transfer coefficient(W/m$^2$-K)

$h_{jet}$ - Back Jet heat transfer coefficient(W/m$^2$-K)

$h_{rad}$ - Radial coolant heat transfer coefficient(W/m$^2$-K)

$h_o$ - Outer heat transfer coefficient(W/m$^2$-K)

$H$ - Boiling Height (m)

$I$ - Proton beam current (μA)

$K_s$ - Thermal Conductivity of Solid (W/m-K)

$K_f$ - Thermal Conductivity of Fluid (W/m-K)

$K_o$ - Constant

$L$ - Characteristic length (m)

$L_i$ - Inlet pipe length

$L_e$ - Exit pipe length

$L_r$ - Radial pipe length

$\dot{m}_r$ - Mass Flow rate in pipe connected to Radial channel manifold (Kg/s)

$\dot{m}_b$ - Mass Flow rate in pipe connected to Back Jet cooling system manifold (Kg/s)

$n_T$ - Number of radial coolant channels

$Nu$ - Nusselt number

$\nu$- kinematic viscosity (m$^2$/s)

*PET* - Positron Emission Tomography

$Pr$ - Prandtl number

$P_e$ - Exit pressure (Pa)

$P_i$ - Inlet pressure (Pa)

$\Delta P$ - Pressure difference between manifolds (Pa)

$Q_{beam}$ - Total Heat Input to Target (W)

$Q_{back}$ - Heat transfer to back due to jet (W)

$Q_{rad}$ - Heat transfer to radial channel (W)

$Q_r$ - Volume flow rate through coolant channels ($m^3/s$)

$Q$ - Volume flow rate through pipe ($m^3/s$)

$\frac{q'''_{avg}}{I}$ - Average volumetric heat generation in Window per unit current

$\frac{q''_{avg}}{I}$ - Average heat flux from Window per unit current

$\frac{q}{I}$ - Average heat from Window per unit current

$q''_{crit}$- Critical Heat flux

$R^{crit}_{pta}$ - Critical peak average ratio

$Ra$ – Rayleigh number

$Re$ – Reynolds number

$\rho$ – Density ($Kg/m^3$)

$\rho_f$ - Liquid density ($Kg/m^3$)

$\rho_g$ - Vapor density ($Kg/m^3$)

$S$ - Jet exit-to-impingement distance (m)

$S / d$ - Ratio of the exit-to-impingement distance to the jet exit diameter

$T$ - Temperature (°C)

$T_{max}$ - Maximum temperature (ºC)

$T_s$ - Solid Temperature (°C)

$T_\infty$ - Ambient Temperature (°C)

$T_{cool}$ - Coolant temperature (°C)

$T_{out,radial}$ - Temperature of coolant at radial channel outlet manifold (°C)

$T_{out,back}$ - Temperature of coolant at back jet outlet manifold (°C)

$T_{sat}$ - Saturation temperature (°C)

$S_{yt}$ - Yield Strength(MPa)

$\mu$ - Dynamic viscosity of liquid (Pa-s)

$V_r$ *or* $v_r$ - Velocity of coolant in radial channel (m/s)

$V$ - Velocity of coolant in pipe connected to manifolds (m/s)

*VECC* - Variable Energy Cyclotron Centre

$x$ - Dryness fraction

# CHAPTER 1

## INTRODUCTION

### 1.1 Background

Positron Emission Tomography (PET) is a radionuclide based functional imaging technique that is used for observing metabolic processes in the body as an aid to diagnose various diseases such as Epilepsy, Cancer, Heart disease, and Alzheimer. PET technique can be combined with a CT scan and MRI to give a better picture of a patient's situation. PET uses FDG (Fluorodeoxyglucose) labeled with $F^{18}$ based radionuclide. Malignant cancerous cells, brain, liver, and kidney consumes glucose at a faster rate leaving $F^{18}$ attached to the cells when it is injected into the body (Phelps,2004). These cells are detected as a bright spot in the PET scanner (Ollinger,1997), exposing the region of growing disease. The physics of FDG is based on a positron($_{+1}e^0$) emission by $F^{18}$ radioisotope ($t_{1/2}$ =110 min), which interacts with human tissues and has a mean range of 0.6 mm in it. It annihilates with electrons present in the cell. Two gamma photons, each with 511 keV energy, which is also the rest mass energy of an electron, are emitted. They travel oppositely in a straight line and get detected by gamma detectors (Valk,2003).

$F^{18}$ is a short-lived radionuclide that is produced by $O^{18}(p,n)F^{18}$ reaction. A cyclotron is used to accelerate proton. The proton energy must be greater than 2.4 MeV energy as it is the threshold energy for the reaction to proceed. This accelerated proton beam must be focused on the small volume of $O^{18}$- Enriched Water. After completion of the reaction, the $F^{18}$ produced is synthesized in FDG. The $F^{18}$ is a short-lived isotope, so the cyclotron must be located close to hospitals having PET scanner (Nuclides,1996). There are two types of liquid target design to produce $F^{18}$

radioisotope. One is recirculating targets and the other is Thermosyphon targets. In recirculating target design, the target heated fluid is allowed to flow through a heat exchanger with the help of a pump, cooled and returned to target chamber (Clark,2004). In Thermosyphon type of targets, which is gravity driven, heat transfer is achieved through transfer of latent heat. The high energy protons lose their kinetic energy into thermal energy, which causes the boiling of the water in a small volume. The increased heat transfer due to the boiling of fluid and absence of non-condensable gas enhances the thermal capacity of the target compared to other batch target designs (Wieland,2002).

Sufficient cooling arrangements are required to avoid over-pressurization of the target chamber and excessive void formation. Over pressurization will lead to rupture of the wall. Moreover, the excessive void formation will allow the proton beam to penetrate the target and strike the back wall. It will reduce the yield of $F^{18}$ due to insufficient interaction between target water and proton beam. There is also a possibility of radiation degradation of the back wall and the alteration of FDG chemistry.

## 1.2 Literature Review

Commercial PET scanners are under development for the past 35 years. Several types of liquid and gas targets had been designed. The two prominent types are re-circulating type and Thermosyphon batch type. Most of the proton energy hitting the liquid is converted to thermal energy. The increase in temperature due to proton bombardment limits the thermal load capacity of the target to 1 kW. Over the last two decades, extensive work has been done to increase the capacity of liquid targets by altering the design and employing different cooling arrangements.

1. Satyamurthy et al. (2002) argue that the target body material, such as silver, has induced activation, which results in poor yield of $F^{18}$. Tantalum can be used as body material because of its chemical inertness and low induced activation. However, its low conductivity imposes a challenge.

2. Roberts et al. (1995) observe that a target consisting of silver body and gold back operating at 40 bar pressure with small liquid volume can produce up to 79% of the theoretical maximum for beam current up to 40 μA.

3. Zeisler et al. (2000) tested small spherical niobium target which give 95% of theoretical yield for $F^{18}$. The result indicated that niobium is excellent material for target construction. The target is irradiated with 21 MeV proton beam, but the target chamber receives 13.1 MeV beam due to loss while passing through cooling water and niobium chamber wall.

4. Stokely (2007) found that the target design with monolithic core, which integrates both the target chamber and radial cooling channels into a single solid piece of tantalum has reduced the conduction thickness significantly. It has also simplified the modelling by removing tantalum/aluminum interface between radial cooling chambers and chamber wall.

5. Berridge et al. (1999) observe good production yields for a double foil, low pressure target with Havar foil window and silver target body at 340 W proton beam power.

6. Bennington et al. (2002) observe good FDG production yield with titanium and niobium based targets. It also eliminated the need for periodic target maintenance.

7. Peeples (2006 & 2008) developed a computational method to support target design and its validation through experiments on targets at different cyclotrons. It was observed that initially,

subcooled boiling occurred followed by turbulent boiling in tantalum-based targets. There was good agreement between experimental data and the volume-averaged boiling model. It had also been observed that critical flux could become an issue for high beam current and low target liquid pressure. Modeling results indicate that the cylindrical target chamber has enhanced thermal performance over racetrack design. For the same heat dissipation, cylindrical targets have a low average void. The same volume of target liquid cylinder has more depth, which increases the thermal limit.

## 1.3 Objectives

The objective of this project work is to develop a computational method for designing Thermosyphon targets. Transient Thermal analysis of target chamber is carried out using ANSYS software package to check the variation of Void Fraction(α) with time and to find Void Fraction(α) value at saturation point of boiling target liquid. Steady State Thermal analysis is done in order to determine maximum temperature in target chamber. This temperature should be under limit to prevent the failure of target chamber during operation. Static Structural analysis is done on Target Window material to check its reliability under pressurized condition. The stress on the Window must be under safe limit to prevent rupture.

## 1.4 Organization of the Thesis

The first part of this chapter gives an overview of background of target design, types of target and application. The second part of this chapter provides information about related work done in target design across the world. The final part describes the objectives of the project work. Chapter 2 explains about different aspects related to Target design such as Material selection, Particle Energy and Heat Input calculation. Chapter 3 describes the modeling of Target chamber and Flow chart of heat transfer distribution in different region. Chapter 4 deals with the lumped system analysis of a closed chamber liquid similar to target chamber. Chapter 5 outlines the detail of critical heat flux, maximum temperature and stress analysis on Target Window. Chapter 6 explains the various steps followed during Finite Element Analysis of Target chamber design. Chapter 7 shows the result obtained during Thermal analysis and Structural stress analysis of target chamber. Chapter 8 provides information regarding conclusion drawn from the analysis and offers recommendations for future work.

# CHAPTER 2

## 2.1 TARGET DESIGN

### 2.1.1 Description

Thermosyphon target is used for producing $F^{18}$ radionuclide for PET scanning. It is a closed chamber filled with pressurized Enriched ($O^{18}$) water having a thin window at the front which allows the proton beam incoming from a cyclotron to pass through it. This proton beam after striking target liquid produces $F^{18}$ radionuclide from $O^{18}$ through nuclear reaction. As the proton beam lose their kinetic energy into thermal energy the temperature of the target chamber increases. Efficient cooling arrangements are required on the radial and the back side of target chamber in order to maintain the temperature at a desired level at steady state. This is constant pressure system with some fixed initial volume of target liquid. To control the pressure inside the target chamber during operation, it will be connected to pressurized buffer tank containing Helium gas, Safety relief valve and a rupture disc through a pipe. When pressure inside the target chamber increases the liquid will expand and it will release the helium gas present in pipe through safety valve. In case the pressure rise is too high, then rupture disk will get punctured. In case the pressure inside the target chamber comes below the desired level, then the buffer tank will supply the Helium gas through pipe to maintain desired pressure in target chamber.

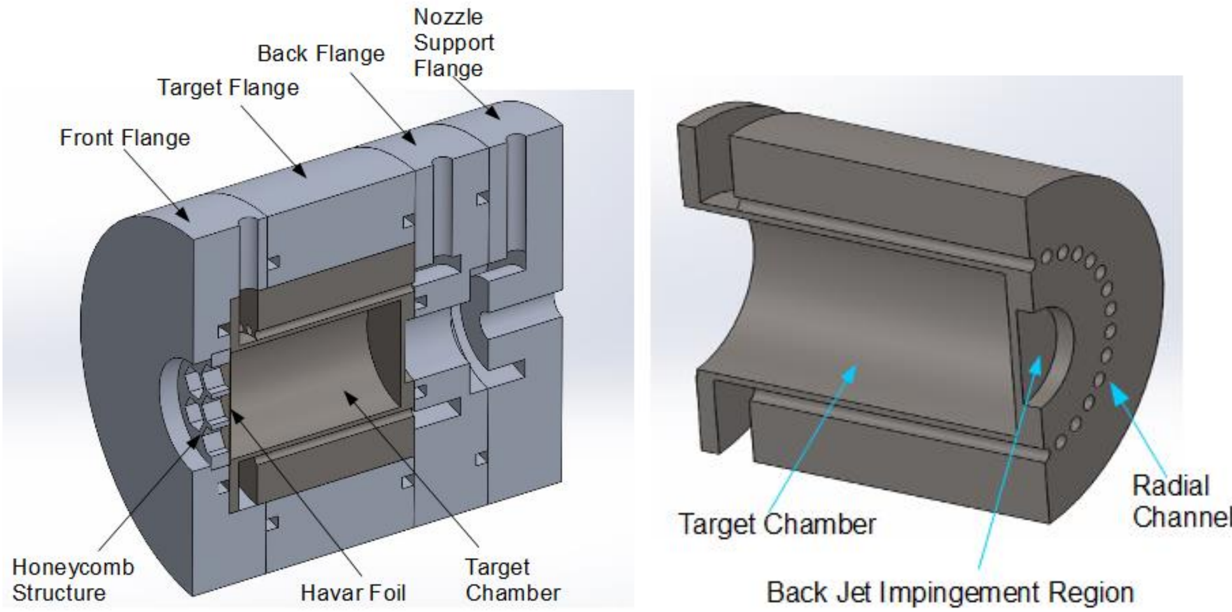


**Figure 1: Target Chamber Pictorial View**

### 2.1.2 Flow Chart

A flow chart representing the steps involved during modeling of target chamber is given in figure-2. It provides details of various parameters considered during target design. Another flow chart showing the procedure for Input heat calculation of target is given in figure-3.

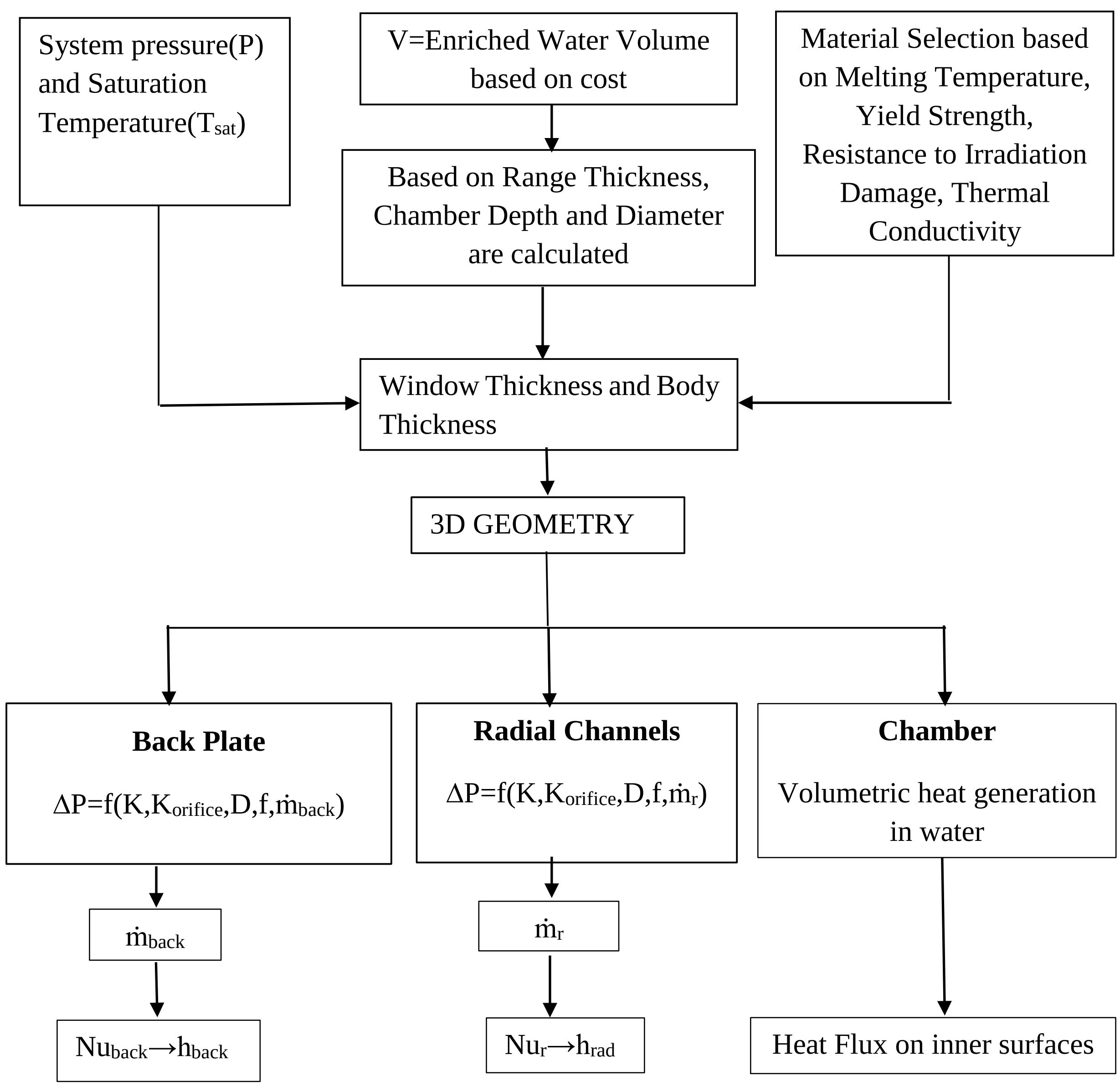


**Figure 2: Flow chart for calculating heat transfer coefficients of different regions**

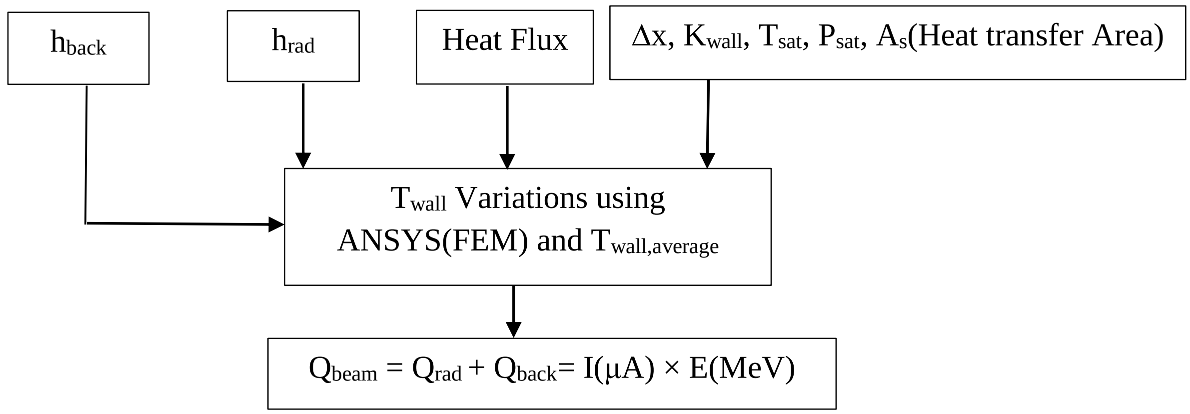


**Figure 3: Flow chart for calculating Heat Input**

### 2.1.3 Materials

The six major components of the Thermosyphon target are Degrader, Sacrificial Grid, Window Support Grid, Window, Target Chamber, and Housing. The degrader reduces the proton beam energy to an energy that is suitable for a nuclear reaction. Material for degrader is essential and depends upon the desired energy required for nuclear reaction and energy of incoming proton beam. The degrader must attenuate the beam effectively by dissipating proton beam energy. Aluminum is a good option because it requires a small thickness to achieve the desired energy loss. It should have good thermal conductivity to dissipate heat quickly.

Target "Window" is a thin metallic foil that allows the proton beam to pass through it with minimum attenuation. So, it must be thin but sufficient to hold the high-pressure target liquid without rupture. Target Window thickness is generally between 10 μm to 200 μm range. It must have high resistance to radiation damage, high mechanical strength, high thermal conductivity, and easy machinability. Good thermal conductivity is preferable as heat will get dissipated quickly.

It should also not chemically contaminate the target water affecting FDG production. Some common materials used in the window are Titanium, Havar, and Tantalum.

The target chamber material's chemical compatibility with chamber liquid is a key concern. High melting point, good thermal conductivity, high material strength, and corrosion resistance are essential parameters. Proton beam interaction with the target chamber internal and window can produce ions that can react chemically with $F^{18}$ ions. It will lead to contamination of target chamber water and reduce $F^{18}$ yield. Nuclear activation due to irradiation is a significant concern during long runs at high beam current (Helus,1987). Common materials for the target chamber are Silver, Tantalum, and Niobium.

Window support grid is a honeycomb structure to support the thin window in case of highly pressurized target design and large window diameter. But, it also reduces the transmissibility of proton beam current. Aluminum can be used for this purpose due to its high thermal conductivity and low cost. Sacrificial grid is identically matches with support grid but precedes it and attenuate the proton beam that would otherwise deposit energy into window support grid, causing unnecessary temperature rise. High thermal conductivity materials like aluminum and copper can be used. The Housing provides structural support to the target chamber and window and aligns them properly on the cyclotron beamline. Housing should be rigid, durable, high strength, good thermal conductivity, and resistance to irradiation damage. In this project work only Window Support Grid, Window, Target Chamber, and Housing is designed.

### 2.1.4 Particle Energy

In cyclotron proton beam are allowed to pass through the target window, where they lose some energy. These protons then lose extra energy during their slowdown in the liquid contained in the target chamber. As more Proton strikes the liquid target, the yield of $F^{18}$ increases. The nuclear cross-section of the reaction first increases to a maximum and then decreases with the energy of the Proton. On the other hand, Saturation Yield keeps on increasing. Saturation yield tells us about the quality of $^{18}F$ production. So, it is beneficial to operate at high incident Proton energy.

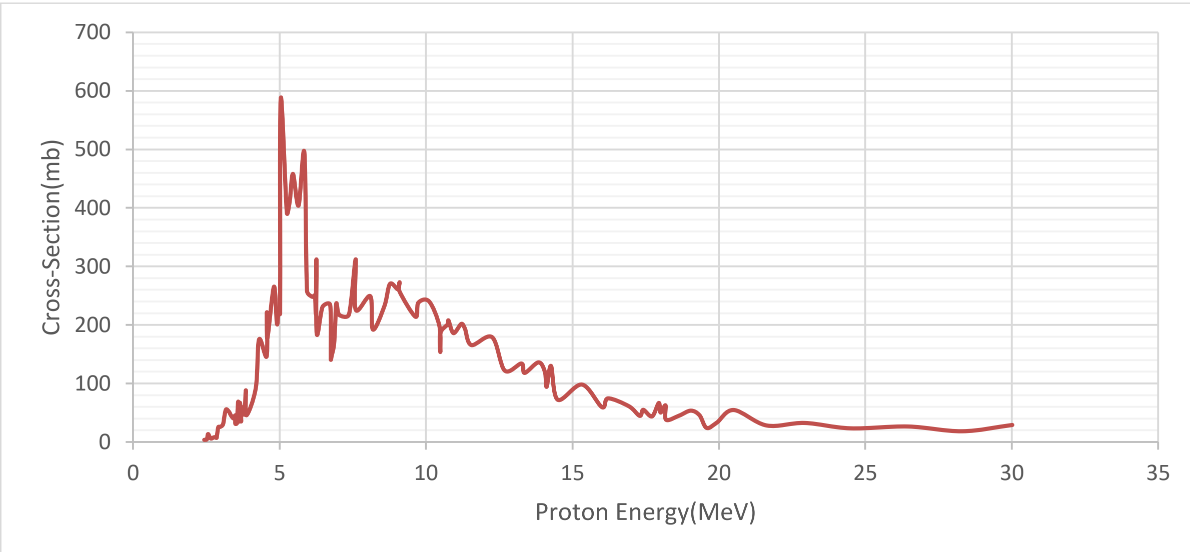


**Figure 4: $^{18}O(p,n)^{18}F$ Nuclear Cross Section. Plot generated from the data of Hess et. al.**

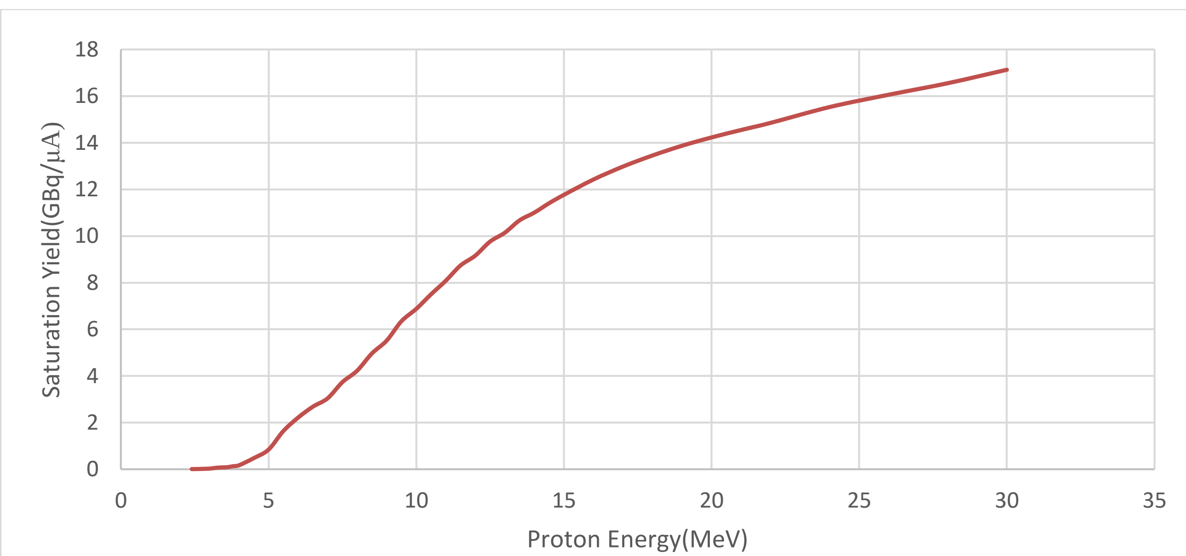


**Figure 5: Saturation Yield in GBq/µA Plot generated from the data of Hess et. al.**

The incremental energy loss per unit length ($\frac{dE}{dx}$) is known as stopping power. Stopping power changes as Proton travels through the water; it attains maximum value known as Bragg peak and suddenly falls to zero. At the Bragg peak amount of energy deposited by Proton is maximum (Faw,1999). The range of Proton is the average distance traveled in the water before being stopped entirely. The high energy deposition reduces density and creates a void in the region. Also, with higher Proton beam energy, the stopping power reduces and beam travel farther in the water before coming to a halt. A higher energy proton sees more $^{18}O$ atom than a lower energy proton, so it results in more yield, as can be seen in the saturation yield plot in Figure 5.

### 2.1.5 Heat Input Calculation

The input heat ($Q_{beam}$) is a function of beam current I(μA) and Proton Energy E(MeV).

It can be expressed as

$$Q_{beam}(\text{Watt}) = I(\mu A) \times E(\text{MeV}) \qquad (2)$$

Generally, E varies between 16MeV to 30MeV. As changing E can vary nuclear cross-section of reaction so $Q_{beam}$ is more dependent on I than E. But we cannot keep increasing 'I' beyond a certain limit, as it may lead to high heat flux and consequently melting of HAVAR foil.

## 2.2 RADIAL COOLANT CHANNELS DESIGN

### 2.2.1 Description

The radial coolant channel's inlet manifold is connected to a supply tank, which delivers coolant to the cyclotron. The VECC facility has a water storage system that provides water of 20 ˚C with a pressure differential between inlet and outlet manifold ΔP as 7 Kg/cm$^2$ (0.68 MPa). A smooth pipe is considered for measuring pressure losses in the Target system. The head loss is due to entry loss, exit loss, radial channel loss, inlet, and outlet manifold loss. Any piping loss apart from these are neglected. The equations for evaluation of the aforementioned losses are given in subsequent section. The radial coolant channels are placed such that radial conduction distance between them and target chamber is 0.5 mm. For a given pressure drop, pipe dimensions and radial channel diameter, heat transfer coefficient and maximum allowable volume flow rate can be calculated. Maximum allowable velocity in piping system should be below 2.4 m/s (Engineering Toolbox,2003) to avoid flow induced vibration. This heat transfer coefficient in radial coolant channel and coolant temperature will give the amount of heat that can be extracted from the target via radial coolant channels.

### 2.2.2 Heat Transfer Coefficient

The heat removal capacity of the radial coolant channels can be calculated using a heat transfer coefficient ($h_{rad}$) and the known coolant fluid temperature. The Dittus-Boelter equation is a well-known correlation for heat transfer coefficients for internal turbulent forced convection flow. The heat transfer coefficient is a function of the Reynolds number and is higher for a higher volume flow rate. For situations where the fluid inside the pipe is being heated by the walls of the pipe via heat flux, the Nusselt number is

$$Nu = 0.023 R_e^{0.8} P_r^{0.4} \qquad \text{(Cengel,2015)}$$

Using the definition of Nusselt No., Reynolds No. and Prandtl No., heat transfer coefficient related to the cooling channel can be expressed as

$$\frac{h_{rad} d_r}{K_f} = 0.023 \left(\frac{\rho Q_r d_r}{\mu A_{rad}}\right)^{0.8} \left(\frac{\mu\, C_f}{K_f}\right)^{0.4} \qquad (1)$$

which reduces to

$$h_{rad} = 0.023\ \frac{K_f}{d_r}\left(\frac{\rho v_r d_r}{\mu}\right)^{0.8}\left(\frac{\mu\, C_f}{K_f}\right)^{0.4} \qquad (2)$$

Figure-6 shows the sectional and side view of target chamber. Water flow direction in Radial channels and Back jet is shown. Niobium and HAVAR foil is also labeled.

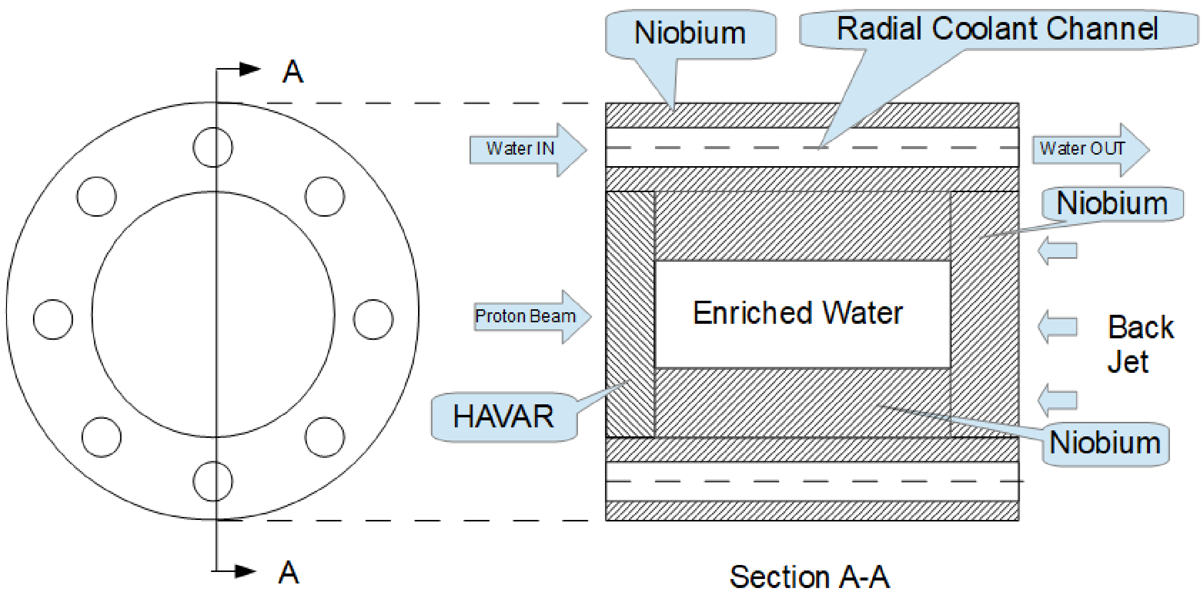


**Figure 6: Front and Side View of Water flow through Radial Coolant Channels**

### 2.2.3 Head Losses

To calculate head losses associated with radial coolant channel, a simplified model shown in Figure-7 is considered.

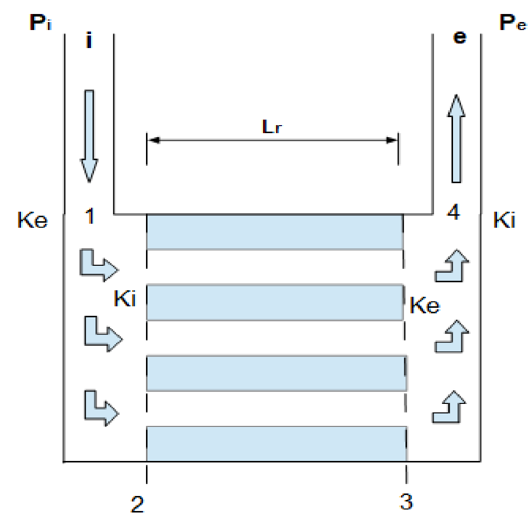


**Figure 7: Water flow through Radial Coolant Channels**

The Head loss associated with each section is represented below:

$$h_{i1} = \frac{f_i L_i V^2}{2D_i g} \tag{3}$$

$$h_1 = \frac{K_e V^2}{2g} \tag{4}$$

$$h_2 = \frac{K_i V_r^2}{2g} \tag{5}$$

$$h_{23} = \frac{f_r L_r V_r^2}{2d_r g} \tag{6}$$

$$h_3 = \frac{K_e V_r^2}{2g} \tag{7}$$

$$h_4 = \frac{K_i V^2}{2g} \tag{8}$$

$$h_{4e} = \frac{f_e L_e V^2}{2D_e g} \tag{9}$$

The sum of equation 3 to 9 is

$$h_L = h_{i1} + h_1 + h_2 + h_{23} + h_3 + h_4 + h_{4e} \tag{10}$$

$$h_L = \frac{f_i L_i V^2}{2D_i g} + \frac{K_e V^2}{2g} + \frac{K_i V_r^2}{2g} + \frac{f_r L_r V_r^2}{2d_r g} + \frac{K_e V_r^2}{2g} + \frac{K_i V^2}{2g} + \frac{f_e L_e V^2}{2D_e g} \tag{11}$$

Friction factor for smooth circular tube, as a function of Reynold's number is

$$f=\begin{cases} \frac{64}{R_e} & R_e < 2000 \\ F(R_e)\ graph & 2000 < R_e < 4000 \\ 0.3164 R_e^{-0.25} & 4000 < R_e < 100000 \end{cases}$$ (I.E. Idelchik, graph of f vs $R_e$)

Data regarding dimensions:

$D_i=D_e=D=12.7$mm (Standard pipe size available), $L_i=L_e=8$ mm, $L_r=17.7$ mm

$$R_e= \left(\frac{\rho Q D}{\mu A}\right),\ Re_r=\left(\frac{\rho Q_r d_r}{\mu A_{rad}}\right),\ Q=n_T Q_r,\ V_r= \frac{Q_r}{A_{rad}},\ V= \frac{Q}{A},\ \rho = \text{constant}$$

The loss coefficient related to sudden contraction of fluid is given by

$$K_i = 0.5\left(1-\frac{A_{small}}{A_{large}}\right)^{0.75}$$ (Idelchik,2008)

For severe restriction in flow area, $\frac{A_{small}}{A_{large}} \rightarrow 0$

This loss coefficient attains maximum value with $K_i=0.5$

The loss coefficient related to sudden expansion of fluid is given by

$$K_e = \left(1-\frac{A_{small}}{A_{large}}\right)^2$$ (Idelchik,2008)

For expansion of fluid to large area, $\frac{A_{small}}{A_{large}} \rightarrow 0$

This loss coefficient attains maximum value with $K_e=1$

Assuming Turbulent flow with 4000<$R_e$<100000 , we can use $f = 0.3164 R_e^{-0.25}$ in the expression of $h_L$

$$h_L = \frac{(L_i+L_e)Q^2}{2D_iA^2g} \times 0.3164\,(\frac{\rho QD}{\mu A})^{-0.25} + \frac{(K_i+K_e)Q^2}{2A^2g} + 0.3164(\frac{\rho QD}{\mu A})^{-0.25} \times \frac{L_rQ_r^2}{2d_rA_{rad}^2g} + \frac{(K_i+K_e)Q_r^2}{2A_{rad}^2g} \quad (12)$$

Equation 12 can be easily substituted in Equation 13

$$h_L = \frac{\Delta P}{\rho g} \quad (13)$$

The above equation is non-linear in Q, and have to be solved for a given value of ΔP. In this project work, based on pressure loss between inlet and outlet manifold (ΔP), radial channel diameter ($d_r$) and number of channels ($n_T$) a radial heat transfer coefficient value ($h_{rad}$) was calculated. The parameters are mentioned in table-1.

**Table 1: Parameters obtained for different Radial channel dimensions**

| ΔP(MPa) | $d_r$(mm) | $n_T$ | $V_r$(m/s) | V(m/s) | $h_{rad}$(W/m$^2$K) |
|---|---|---|---|---|---|
| 0.1 | 0.5 | 40 | 8.25 | 0.511 | 46912 |
| | 1 | 28 | 9.69 | 1.682 | 46449 |
| | 2 | 16 | 10.04 | 3.98 | 41600 |

## 2.3 JET COOLING SYSTEM DESIGN

### 2.3.1 Description

As there are no cooling channels at the back of the target, a jet impingement cooling system is used. The jet flow system is maintained at a pressure differential of 7 Kg/cm$^2$ (0.68 MPa) between inlet and outlet manifold. The head loss is due to entry loss, exit loss, contraction loss, inlet, and outlet manifold loss. Any piping loss apart from these are neglected. The equations for evaluation of the aforementioned losses are given below. For a given pressure loss, the volume flow rate and heat transfer coefficient can be calculated. This heat transfer coefficient at back and coolant temperature will give the amount of heat that can be extracted from the target via Jet cooling at the back.

### 2.3.2 Heat Transfer Coefficient

For submerged jet water with $2 \leq S/d \leq 12$, $5 \leq D_{imp}/d \leq 15$, $2000 \leq Re_d \leq 400000$

$$h_{jet} = \frac{K_f}{D_{imp}} \frac{\left[2-4.4\left(\frac{d}{D_{imp}}\right)\right]}{\left[1+0.2\left(\left(\frac{S}{d}\right)-6\right)\left(\frac{d}{D_{imp}}\right)\right]} 2Re_d^{0.5}\left[1+\frac{Re_d^{0.55}}{200}\right]^{0.5} Pr_f^{0.42} \quad \text{(Martin,1977)} \qquad (1)$$

The geometry configuration, which resulted in maximum heat removal, is $\frac{S}{d} = 2$ and $\frac{D_{imp}}{d} = 5$ (Peeples,2006). A given target chamber height would specify the value of $D_{imp}$, and the values of S and d could be selected using these optimized ratios.

### 2.3.3 Head Losses

To calculate head losses associated with Jet cooling system, a simplified model shown in Figure-8 is considered.

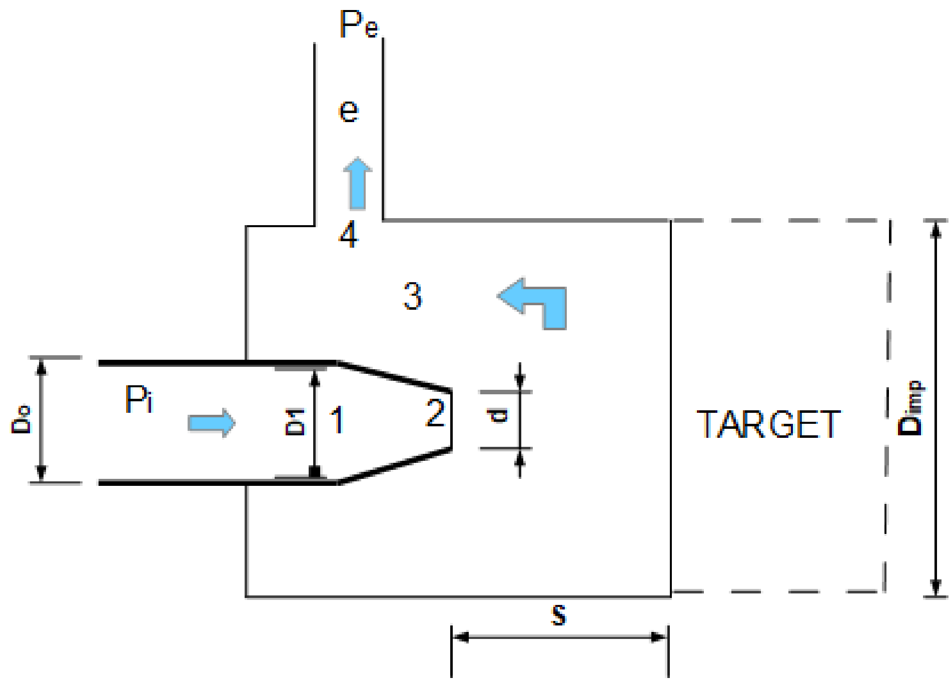


**Figure 8: Water Flow through Jet Cooling System**

The Head loss associated with each section is represented below:

$$h_{i1} = \frac{f_i L_i V^2}{2D_i g} \tag{2}$$

$$h_2 = \frac{K_n {V_2}^2}{2g} \tag{3}$$

$$h_{baffle} = \frac{K_{baffle} V_2^2}{2g} \tag{4}$$

$$h_{23} = \frac{K_{90} V_3^2}{2g} \tag{5}$$

$$h_4 = \frac{K_i V^2}{2g} \tag{6}$$

$$h_{4e} = \frac{f_e L_e V^2}{2D_e g} \tag{7}$$

The sum of equation 2 to 7 is

$$h_L = h_{i1} + h_2 + h_{baffle} + h_{23} + h_4 + h_{4e} \quad (8)$$

$$h_L = \frac{f_i L_i V^2}{2D_i g} + \frac{K_n {V_2}^2}{2g} + \frac{K_{baffle} V_2^2}{2g} + \frac{K_{90} V_3^2}{2g} + \frac{K_i V^2}{2g} + \frac{f_e L_e V^2}{2D_e g} \quad (9)$$

Friction factor for smooth circular tube, as a function of Reynold's number is

$$f=\begin{cases} \frac{64}{R_e} & R_e < 2000 \\ F(R_e)\ graph & 2000 < R_e < 4000 \\ 0.3164R_e^{-0.25} & 4000 < R_e < 100000 \end{cases}$$ (I.E. Idelchik, graph of f vs $R_e$)

Data regarding dimensions:

$D_i=D_e=D_1=D_4=D$, $L_i=L_e$ , $R_e= (\frac{\rho Q D}{\mu A})$, $V_2= \frac{Q}{A_2}$ , $V_3= \frac{Q}{A_3}$ ,$V= \frac{Q}{A_1}$ , $\rho$= constant , $f_i = f_e$

Area associated with region 3 is given by

$$A_3 = \frac{\pi}{4} D_{imp}^2 - \frac{\pi}{4} d^2 \quad (10)$$

The loss coefficient related to sudden contraction of fluid is given by

$$K_i = 0.5(1 - \frac{A_{small}}{A_{large}})^{0.75}$$ (Idelchik,2008)

For severe restriction in flow area, $\frac{A_{small}}{A_{large}} \to 0$

This loss coefficient attains maximum value with $K_i$=0.5

The loss coefficient related to nozzle is given by

$$K_n = (1 - (\frac{d}{D})^4) \quad (11)$$

Form loss coefficient associated with jetting of fluid on baffle is given by

$K_{baffle}=1$ (Idelchik,2008)

Form loss coefficient associated with 90˚ turn is given by

$K_{90}=1$ (Idelchik,2008)

Assuming Turbulent flow with 4000<$R_e$<100000 , we can use $f = 0.3164R_e^{-0.25}$ in the expression of $h_L$ .

$$h_L = \frac{(L_i+L_e)Q^2}{2D_iA^2g} \times 0.3164(\frac{\rho QD}{\mu A})^{-0.25} + \frac{(K_i)Q^2}{2A^2g} + \frac{(K_n)Q^2}{2A_2^2g} + \frac{(K_{baffle})Q^2}{2A_2^2g} + \frac{(K_{90})Q^2}{2A_3^2g} \quad (12)$$

Equation 12 can be easily substituted in Equation 13

$$h_L = \frac{\Delta P}{\rho g} \quad (13)$$

The above equation is non-linear in Q, and have to be solved for a given value of ΔP.

# CHAPTER 3

## TARGET CHAMBER MODELLING

### 3.1 Description

When heat is deposited in the liquid inside the chamber, boiling takes place. So a turbulent, boiling regime forms. This generates void fraction inside the chamber. With the given cooling rate and heat input, a steady-state void fraction can be achieved. The Correlation for the boiling heat transfer coefficient was applied to only curved surface and back surface inside target chamber region. Boiling heat transfer coefficient is a function of Void fraction. Moreover, this heat transfer coefficient will give temperature distribution in chamber at different void fractions. The heat transfer coefficient between window and chamber liquid is neglected. This is because of high temperature of window, the heat transfer mechanism between window and chamber liquid will be different from other regions inside chamber. Also, this results in a conservative design.

### 3.2 Heat Transfer Coefficient

The Nusselt number for volumetrically heated pools is often correlated in the form (Wen, 2006)

$$N_u = C\mathrm{Ra}^{\mathrm{n}} \tag{1}$$

$$N_u = \begin{cases} 1.54Ra^{0.25}, & Ra \leq 1.865 \times 10^{11} \\ 0.0314Ra^{0.4}, & Ra \geq 1.865 \times 10^{11} \end{cases}$$

$$R_a = \frac{g\alpha H^3 Pr_f}{\nu_f^2} \tag{2}$$

$$Pr_f = \frac{\mu\, c_f}{K_f} \tag{3}$$

$$\nu_f = \frac{\mu}{\rho_f} \tag{4}$$

$$h_{boil} = \frac{K_f}{H} Nu \tag{5}$$

### 3.3 Total Heat Transfer Rate

Total heat transferred out of the target chamber is the sum of the heat transferred radially out to the radial coolant channels, and the heat transferred out of the back of the target to the jet. This heat transfer is equal to the heat input from the proton beam at steady state.

The heat balance is given by

$$Q_{beam} = Q_{rad} + Q_{back} = Q_1 + Q_2 + Q_3 \tag{6}$$

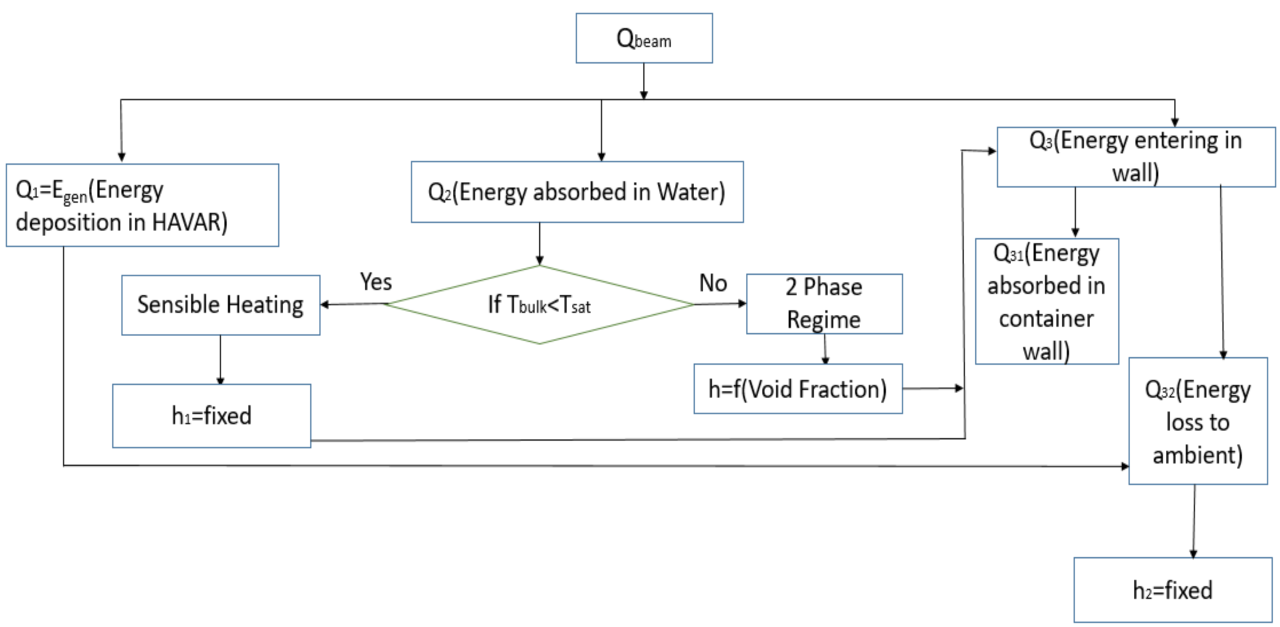


**Figure 9: Flow Chart representing heat transfer distribution in different region**

At steady state all stored heat energy will be zero, i.e., $Q_2 = Q_{31} = 0$

We will model the 1/4th part of chamber by applying constant heat flux on area $A_1$ and $A_2$. Also, we assume that the volumetric heat generation in water will get transferred through area $A_1$ & $A_2$. There will be no transfer of this heat to window foil.

$$q''_{flux} = \frac{Q_{beam} - Q_1}{A_1 + A_2}$$

$$h_{boil,steady\ state} = \frac{q''_{flux}}{T_{sat} - T_{mean}}$$

where $T_{mean}$ is mean temperature of area $A_1$ & $A_2$ at steady state.

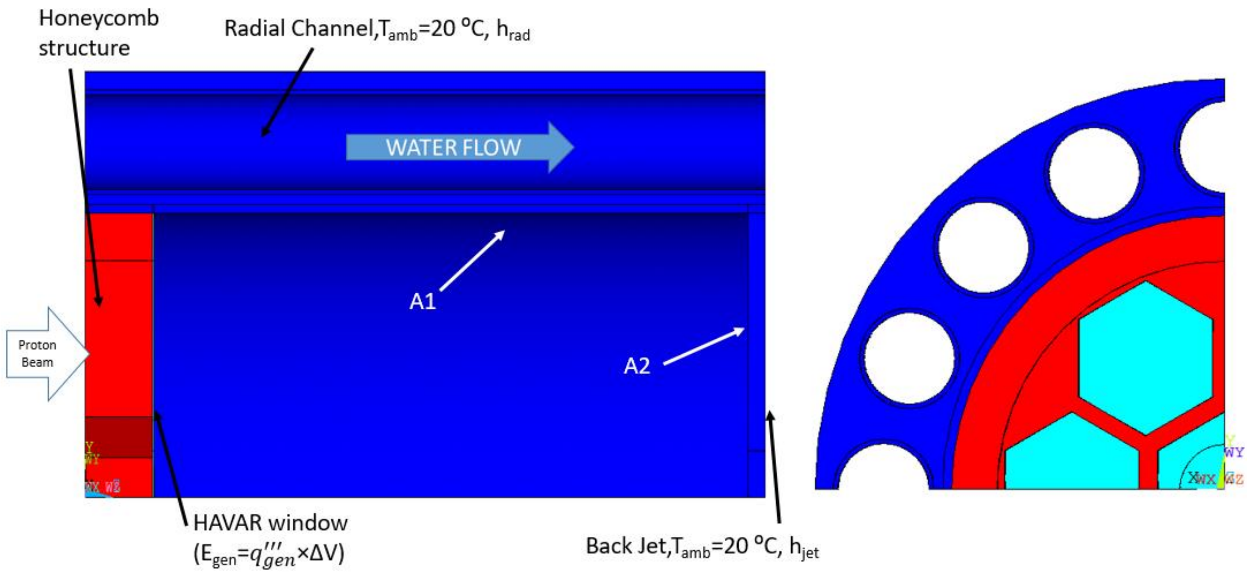


**Figure 10: Sectional and Front view of 1/4th part of target chamber**

# CHAPTER 4

## LUMPED SYSTEM ANALYSIS

### 4.1 Overview

The temperature of a body varies under a thermal load with time and space. In lumped system analysis, the temperature of the body varies with time but remains the same throughout the body at any instant of time. We are considering a closed system where heat will be dumped. The variation of temperature of fluid and solid with time will be analyzed. The water will heat up sensibly, and after attaining a saturation point, it will start boiling. The volume of water taken is 2 mL which is same as Enriched water volume considered in actual target design.

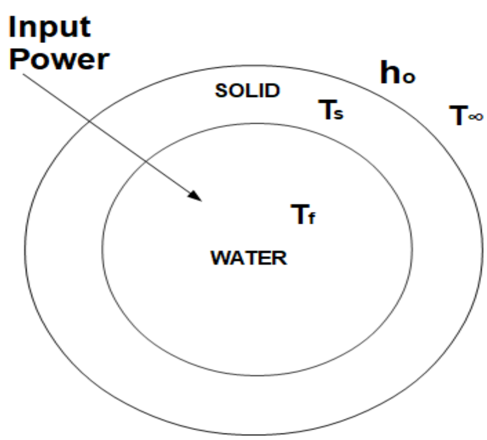


**Figure 11: Lumped two body system with input energy**

*Following Assumptions is considered during Lumped System Analysis:*

1. The fluid was considered as static during operation without any convection current and the only mode of heat transfer inside target chamber is pure conduction. For pure conduction case $N_u = 1 = \frac{h_i D}{K_f}$ is considered.

2. Temperature of fluid and solid is assumed as function of time only.

3. $h_o$ assumed to remain constant and uniform throughout.

The general Energy balance equations for solid and water when sensible heating exist is given by

Heat Input rate - Heat Output rate = Heat Stored rate

$$EI - h_i A_i (T_f - T_s) = \frac{\partial (m_f c_f T_f)}{\partial t} \tag{1}$$

which reduces to

$$EI - \frac{K_f}{D} A_i (T_f - T_s) = \rho_f c_f V_f \frac{\partial T_f}{\partial t} \tag{2}$$

and

$$h_i A_i (T_f - T_s) - h_o A_o (T_s - T_\infty) = \rho_s c_s V_s \frac{\partial T_s}{\partial t} \tag{3}$$

which reduces to

$$\frac{K_f}{D} A_i (T_f - T_s) - h_o A_o (T_s - T_\infty) = \rho_s c_s V_s \frac{\partial T_s}{\partial t} \tag{4}$$

The general Energy balance equations for solid and water when boiling started is given by

Heat Input rate - Heat Output rate = Heat Stored rate

$$EI - h_{boil} A_i (T_{sat} - T_s) = \frac{\partial H}{\partial t} \tag{5}$$

which reduces to

$$EI - K_o A_i \, \alpha^{0.25} (T_{sat} - T_s) = m h_{fg} \frac{\partial x}{\partial t} \tag{6}$$

and

$$h_{boil}A_i(T_{sat} - T_s) - h_oA_o(T_s - T_\infty) = \frac{\partial(m_sc_sT_s)}{\partial t} \qquad (7)$$

which reduces to

$$K_oA_i\,\alpha^{0.25}(T_{sat} - T_s) - h_oA_o(T_s - T_\infty) = \rho_sc_sV_s\,\frac{\partial T_s}{\partial t} \qquad (8)$$

Relation between Void Fraction and Dryness Fraction:

$$\alpha = \frac{1}{\frac{\rho_g}{\rho_f}\left(\frac{1}{x}-1\right)+1} \qquad \text{(Ghiaasiaan,2008)} \qquad (9)$$

By using numerical technique, the equation was solved and variation of different parameters with time was plotted.

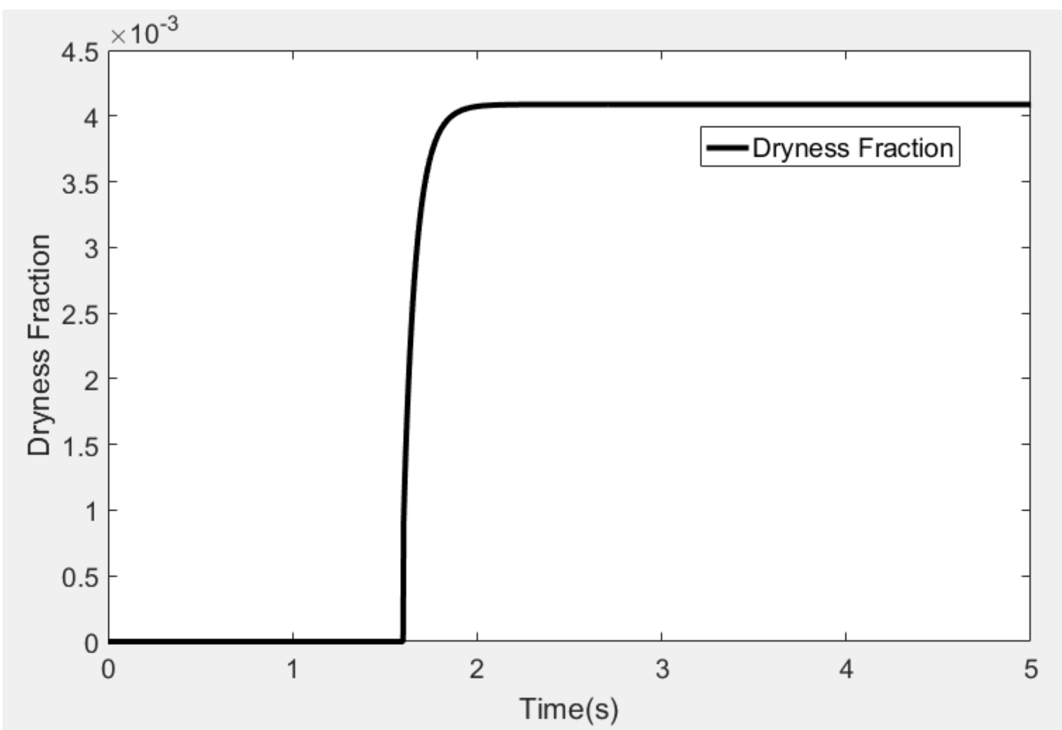


**Figure 12: Variation of Dryness Fraction(x) with time(s)**

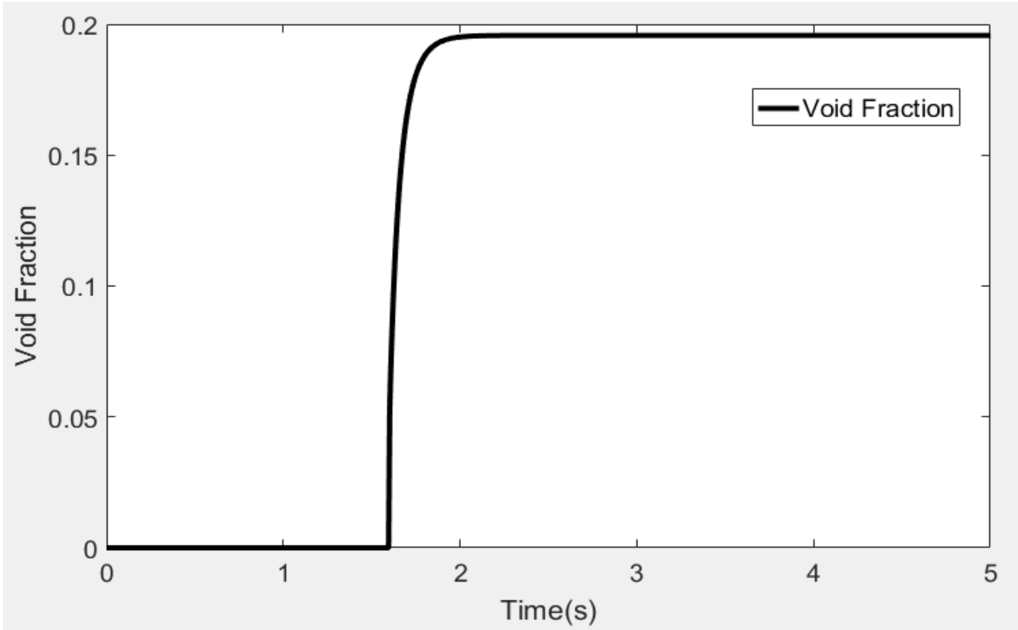


**Figure 13: Variation of Void Fraction(α) with time(s)**

Our lumped analysis (Case 1) considers a hypothetical scenario in which the incident beam energy is first dumped into the target water inventory inside the sphere. Initially the water and solid mass are both at ambient temperature. Once the beam starts hitting the water, sensible heating of water will occur when the temperature will rise from the ambient temperature to the saturation temperature corresponding to the pressure inside the chamber. Please note that since this is a lumped analysis, the temperature gradient within water from the centre of sphere to the water-solid boundary and also within solid wall are neglected. The heat transfer coefficient at water-solid interface during this sensible heating phase is found to be very low (~ 40 $W/m^2K$) assuming Nusselt number equal to unity (pure conduction). This low heat transfer coefficient has increased the thermal resistance between water-solid boundary causing hardly any heat flow to the solid wall. This explains the nearly flat line of temperature of solid during the sensible heating in water given in Figure 14 (Solid lumped case1).

Once the water reaches the two-phase regime, its temperature will remain constant at $T_{sat}$. However, owing to the boiling in water, the heat transfer coefficient between solid-water interface has increased manifold times (~ 2000 $W/m^2K$). This allows heat flow to the solid wall. The temperature of solid has now sharply jumped to a higher value (~ 50 °C) in order to allow the heat transfer to the ambient to take place. The solid temperature is also seen to remain constant at this high value since the void fraction of water has reached steady state as given in Figure 13.

Another lumped scenario (Case 2) is considered taking a high hypothetical heat transfer coefficient in water (~ 1200 $W/m^2K$) instead of pure conduction during the sensible heating phase. In this case, the heat flow from water to solid is happening during the sensible heating phase resulting in a gradual rise in temperature of solid as evident from the Figure 14 (Solid Lumped case 2). The final temperature of solid however, has remained same since the steady state void fraction in water is found to be similar to the earlier lumped case 1.

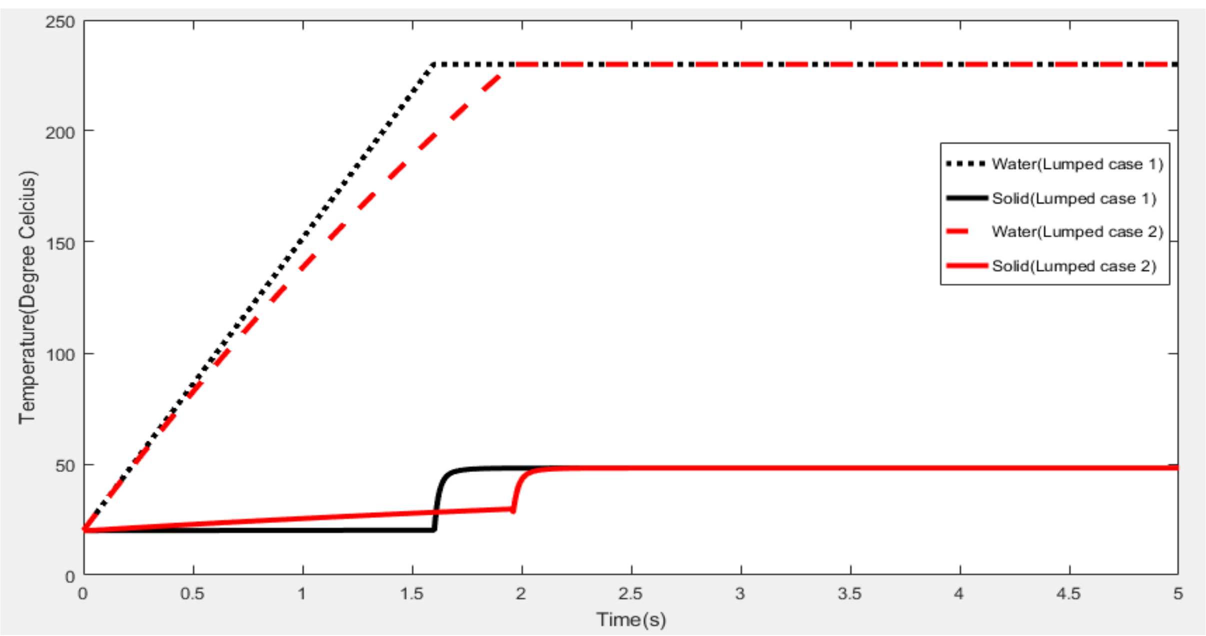


**Figure 14: Variation of Temperature(˚C) of the water and solid with time(s) for 2 different Lumped cases**

## 4.2 Code Description

An OCTAVE code was written which includes the Energy Conservation equations. The differential equation obtained is solved using Euler's Method with initial guess values. The solution converges to some finite value and system attains steady state. The results obtained are plotted in Figure-12, 13 & 14.

# CHAPTER 5

## 5.1 HEAT FLUX AND MAXIMUM TEMPERATURE ON THE WINDOW FOIL

### 5.1.1 Description

Proton beam passing through thin window foil deposits energy inside it, which increases its temperature. The window foil can be considered as insulated at one end and is cooled by enriched chamber water on the other end. Because one end is facing the vacuum side and has very small area, so a very small radiation heat transfer will occur. When the temperature of chamber water reaches saturation point then pool boiling occurs. The heat transfer to the boiling water can be assumed as constant heat flux condition. The boiling water undergoes through different boiling regimes such as natural convection boiling, nucleate boiling, transition boiling and film boiling. Nucleate boiling regime is most desirable as it has highest heat transfer coefficient. During nucleate boiling, isolated bubbles form at nucleation sites, often surface defects, and grow on the surface until their buoyancy forces exceed the surface tension. In nucleate boiling regime there is maximum limit for heat flux known as critical heat flux beyond which the surface temperature of window foil will suddenly become very high. This situation occurs because of vapor blanket formation on the surface which has poor heat transfer compared to boiling liquid.

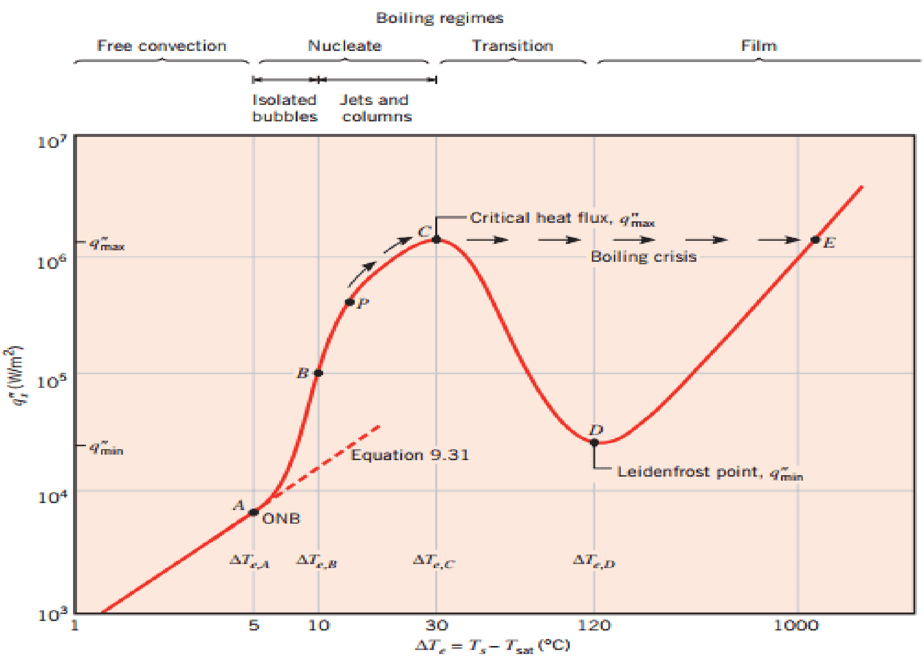


**Figure 15: Boiling Curve for water at 1 atmospheric pressure (Incropera,2011)**

### 5.1.2 Maximum Temperature of Window Foil

Window foil materials are chosen such that it can sustain high temperature without meltdown. But when the heat flux increases beyond critical value, the boiling regimes shift to film boiling region from nucleate boiling region. This results in increased temperature of window foil. High temperature above 40% of melting point leads to degradation of foil material. In some case it results in hole due to melting of window. To avoid such scenario necessary modification must be adopted such as efficient helium gas cooling from vacuum side and minimizing thickness of window foil that results in decrease of energy deposition.

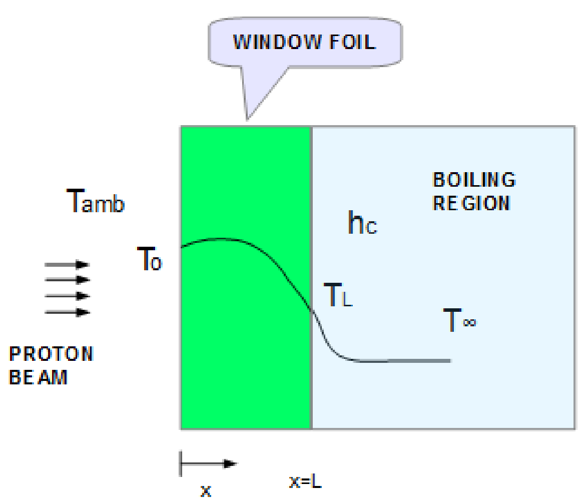


**Figure 16: Sectional view of Target Chamber showing Temperature variation**

Fourier law of heat conduction assuming 1D heat transfer for window foil material is given by

$$\frac{d}{dx}\left(k\frac{dT}{dx}\right) + q'''(x) = 0 \qquad (1)$$

Radiation boundary condition assumed on the sides where proton beam is entering is given by

$$k\left(\frac{dT}{dx}\right)_{x=o} = \sigma\varepsilon(T_o^4 - T_{amb}^4) \qquad (2)$$

where $\sigma$=5.67×10$^{-8}$ $\frac{W}{m^2-K^4}$ and 'ε' is the surface emissivity.

Convective boundary condition on target chamber liquid side is given by

$$k\left(\frac{dT}{dx}\right)_{x=L} = -h_c(T_L - T_\infty) \qquad (3)$$

The conduction equation is integrated along the length to obtain

$$\int_0^x \frac{d}{dx}\left(k\frac{dT}{dx}\right)dx + \int_0^x q'''(x)dx = 0 \qquad (4)$$

Which yields

$$k\left(\frac{dT}{dx}\right)_{x=x} - k\left(\frac{dT}{dx}\right)_{x=0} + \int_0^x q'''(x)dx = 0 \qquad (5)$$

Using equation 2 and equation 3 in equation 5 gives

$$-h_c(T_L - T_\infty) - \sigma\varepsilon(T_o^4 - T_{amb}^4) + \int_0^L q'''(x)dx = 0 \qquad (6)$$

Using equation 2 in equation 5 and integrating along the length to yield

$$\int_0^L k\left(\frac{dT}{dx}\right)_{x=x} . dx - \int_0^L \sigma\varepsilon(T_o^4 - T_{amb}^4) . dx + \int_0^L \int_0^x q'''(x)dx. dx = 0 \qquad (7)$$

This reduces to

$$T_L - T_0 - \frac{\sigma\varepsilon(T_o^4 - T_{amb}^4)L}{k} + \frac{1}{k}\int_0^L \int_0^x q'''(x)dx. dx = 0 \qquad (8)$$

Using equation 2 in equation 5 and integrating along any arbitrary length x the length yields

$$T_x - T_0 - \frac{\sigma\varepsilon(T_o^4 - T_{amb}^4)x}{k} + \frac{1}{k}\int_0^x \int_0^x q'''(x)dx. dx = 0 \qquad (9)$$

Differentiating equation 9 w.r.t 'x' and equating $\frac{dT_x}{dx}$ to zero will give location maximum temperature

$$-\sigma\varepsilon(T_o^4 - T_{amb}^4) + \int_0^{x_{max}} q'''(x)dx = 0 \qquad (10)$$

The convective heat transfer coefficient of target chamber is function of boiling regime and wall temperature. Volumetric heat generation can be considered to be uniform throughout the window. Equation 6 and 8 are non-linear equation with variables as $T_L$ and $T_0$ that can be solved. Equation 9 and 10 will give maximum temperature and its location.

### 5.1.3 Critical Heat Flux Correlation

Critical heat flux correlation for flat vertical plate with one side insulated is given by

$$\frac{q''_{crit}}{q''_{max_z}} = \begin{cases} 0.9 & 5.86 < Bo \\ \frac{1.4}{(H')^{\frac{1}{4}}} & 0.15 < Bo < 5.86 \end{cases}$$

$$H' = L\sqrt{\frac{g(\rho_f - \rho_g)}{\sigma}} \qquad \text{(Dimensionless quantity)}$$

Bond Number is the ratio of gravitational force to the surface tension, is given by

$$Bo = \frac{gL^2(\rho_f - \rho_g)}{\sigma}$$

The Zuber-Kutateladze correlation for critical heat flux on a flat plate is given by

$$q''_{max_z} = \frac{\pi}{24} h_{fg} \rho_g^{0.5} \left[\sigma g(\rho_f - \rho_g)\right]^{0.25}$$

**Table 2: Critical Heat Flux at 400 psia pressure of target liquid**

| | |
|---|---|
| $\boldsymbol{H'}$ | 5.16 |
| $\boldsymbol{Bo}$ | 26.68 |
| $\boldsymbol{q''_{max_z}}$ **(MW/m²)** | 3.47 |
| $\boldsymbol{q''_{crit}}$ **(MW/m²)** | 3.123 |

In Medical cyclotron proton beams with some initial energy can be considered as circular in shape. This beam will deposit its energy in Havar foil that can be estimated using SRIM(Stokely,2008) and other geometrical data provided below.

Beam Energy, $E_{beam}$= 22MeV

Beam Radius= 5 mm

Proton Beam Area, $A_{beam}$= 78.53 mm$^2$

Havar foil thickness, $\Delta x$= 50 µm

Proton beam flux, φ= 1.24×10$^{13}$ $\frac{protons}{cm^2-s-\mu A}$

The Stopping power ($\frac{\partial \mathrm{E}}{\partial \mathrm{x}}$) for a given material and proton beam energy can be calculated by using SRIM.

Average volumetric heat generation in Window per unit current ($\frac{q'''_{avg}}{I}$) can be obtained as

$$\frac{q'''_{avg}}{I} = \frac{\partial \mathrm{E}}{\partial \mathrm{x}} \times \varphi$$

Average heat flux from Window per unit current ($\frac{q''_{avg}}{I}$) is given by

$$\frac{q''_{avg}}{I} = \frac{q'''_{avg}}{I} \times \Delta x$$

Average heat from Window per unit current $\left(\frac{q}{I}\right)$ is given by

$$\frac{q}{I} = \frac{q''_{avg}}{I} \times A_{beam}$$

**Table 3: Heat Generation in 50 µm HAVAR foil (Stokely, 2008)**

| $E_{beam}$(*MeV*) | $\frac{\partial \mathrm{E}}{\partial \mathrm{x}}$ (*MeV/mm*) | $\frac{q'''_{avg}}{I}(W/cm^3\mu A)$ | $\frac{q''_{avg}}{I}(W/cm^2\mu A)$ | $\frac{q}{I}(W/\mu A)$ |
|---|---|---|---|---|
| 22 | 12.89 | 256.05 | 1.28025 | 1.004 |

**Table 4: Critical to average peak ratio for Target at 400 psia**

| $q''_{crit}(W/cm^2)$ | I($\mu A$) | $q''_{avg}(W/cm^2)$ | $R^{crit}_{pta}$ |
|---|---|---|---|
| 312.3 | 50 | 64.01 | 4.9 |
| | 100 | 128.025 | 2.45 |
| | 150 | 192.03 | 1.61 |

Critical peak to average ratio ( $R^{crit}_{pta}$ ) around 5 indicates that the heat flux in window foil will not exceed the critical heat flux value under normal operating conditions. $q''_{avg}$ is a function of parameters such as Beam current, Beam flux, Beam energy, Beam area, Foil thickness and Foil material properties. In order to keep $R_{pta}^{crit}$ within safe limit these parameters must be selected accordingly.

## 5.2 THEORETICAL STRESS ANALYSIS OF THE TARGET CHAMBER

The target chamber used for production of FDG is cylindrical in shape. It is internally pressurized and is placed inside the housing. Due to high internal pressure, there is chance of rupture in the Window as it is only supported through edges. To avoid it, safety analysis of window must be carried out. The Window of target chamber can be considered as circular plate under uniform loading with clamped edge. There will be variation of tangential stress and radial stress along radial direction. The maximum stress will be radial stress at the boundary and is given by

$$(\sigma_r)_{max} = \frac{3}{4}\frac{pR^2}{t^2} \qquad \text{(Timoshenko,2010)}$$

where 'p' is load applied per unit area, 't' is thickness of plate and 'R' is radius of plate.

**Table 5: Radial stress variation with different diameter under uniform loading**

| Pressure(psi) | Thickness (μm) | Diameter(mm) | $(\sigma_r)_{max}$ (MPa) |
|---|---|---|---|
| 400 | 50 | 12 | 29786.4 |
| | | 10 | 20685 |
| | | 8 | 13238.4 |
| | | 6 | 7446.6 |
| | | 4 | 3309.6 |
| | | 2 | 827.4 |

Table-5 shows that maximum stress on a uniformly loaded circular plate with fixed edges and same thickness will decrease by decreasing diameter. So it is better to select smaller diameter Target window. But with decreasing Window's diameter, proton beam size should also be decreased in order to properly utilize the proton beam. This will result in high heat flux on Window surface. The other option is to use Honeycomb support grid to support the window.

**Table 6: Typical tensile mechanical properties of HAVAR in different metallurgical states (Hamilton Precision Metals)**

| Property | Annealed | Cold Rolled(85%) | Cold Rolled & Heat Treated |
|---|---|---|---|
| **$S_{UTS}$(MPa)** | 960 | 1860 | 2275 |
| **$S_{YT}$(MPa)** | 480 | 1725 | 2070 |
| **Modulus of Elasticity(GPa)** | 200 | 200 | 200 |

From Table-6, it is evident that Cold rolled & Heat treated Havar will provide sufficiently higher yield strength.

# CHAPTER 6

## FINITE ELEMENT ANALYSIS

FEM is a method to solve complex real world problems that are not solvable by the traditional method. Finite element models are mathematical representation of the real system. In FEM, a physical model is discretized into many parts known as element. A mathematical equation is obtained for each element, and they are assembled to form a matrix. Essential loads and boundary conditions are applied. The matrix is solved to determine the field variable (such as deformation, stress, temperature, etc.) variation. There are many FEM Analysis commercial software packages available such as ANSYS, ABAQUS, etc. In this analysis, ANSYS is used.

### 6.1 Modeling

An ANSYS 3D model is created to represent the Target Window and Target Chamber. Due to symmetry of problem along z axis, only 1/4$^{th}$ part is modeled. It will reduce the CPU computational time with same result as of full model.

### 6.2 Element Assignment

In ANSYS software, more than 100 different elements are available to model the object. SOLID90 20 nodes brick (Hexahedral) element is used for modeling Target window and Target Chamber for Thermal analysis. SOLID90 is a 3D solid thermal element. It can tolerate irregular shapes without as much loss of accuracy in results. SOLID90 elements have compatible displacement shapes and are well suited to model curved boundaries. It only has Temperature as its Degree of Freedom.

SURF 152 element is used in various load and surface effect application. It is applicable to 3D thermal analysis. Here it is used to calculate heat transfer taking place from given surface.

ANSYS workbench is used for Structural safety analysis of Target Window under pressurized condition. It uses SOLID 186 element, which is a solid structural element. It is well suited for modeling irregular mesh. It has $U_x$, $U_y$ and $U_z$ as Degree of Freedoms. Both SOLID 90 & SOLID 186 have equivalent geometry.

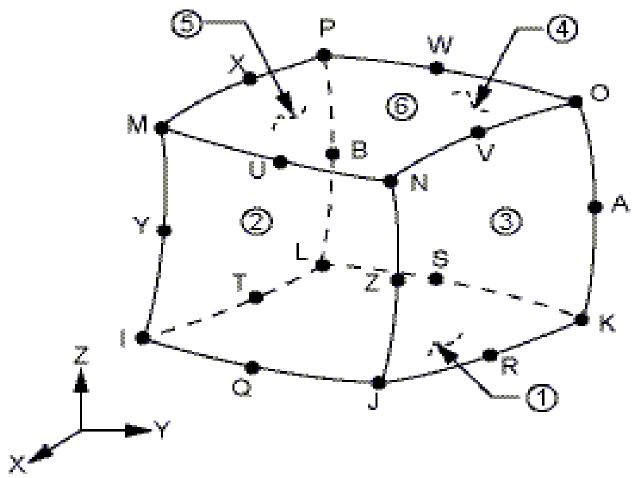


**Figure 17: SOLID 90 & SOLID 186 Element Geometry**

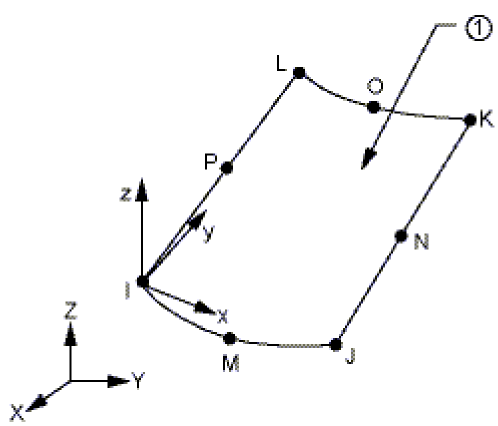


**Figure 18: SURF 152 Element Geometry**

## 6.3 Meshing

Meshing is discretization of continuous body into finite number of elements. It is one of the most important aspects of FEM Analysis. The accuracy of the results depends upon mesh size and quality. More the number of mesh greater is the difficulty in solving problems. Therefore, a preferred meshing approach is to employ fine meshes only in the area of interest and larger meshes should be used in the region where we have relatively less interest.

For Target chamber and Target window model, whole geometry is divided into different regions. Each region is meshed separately with required elements. Generally, irregular geometry does not meet hexahedral meshing criteria, so they are meshed with 10-noded tetrahedral element.

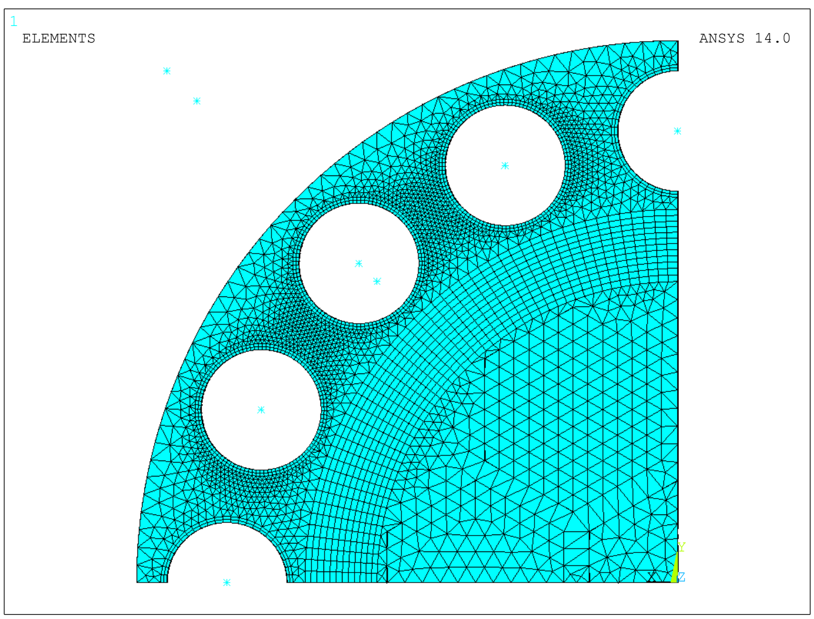


**Figure 19: Front view of Meshed Target Chamber**

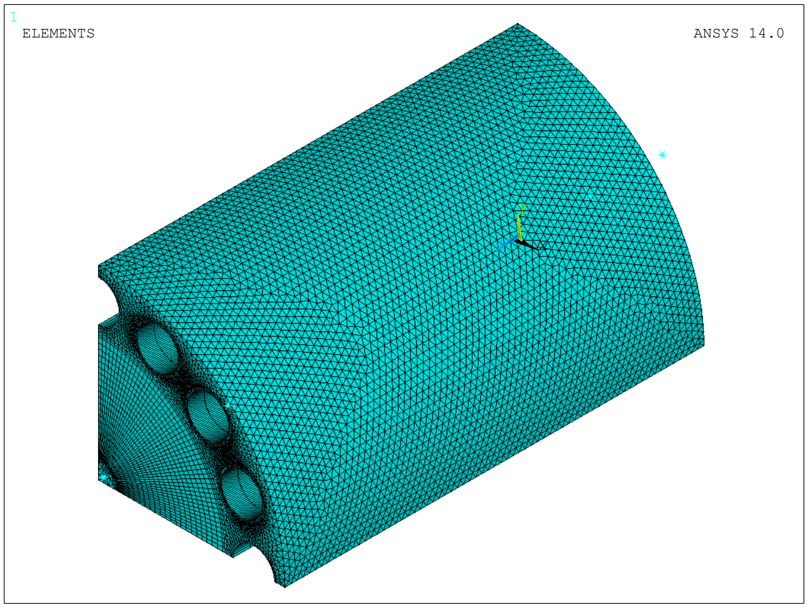


**Figure 20: Isometric View of Meshed Target Chamber**

## 6.4 Loading Conditions and Boundary Conditions

***For Thermal Analysis:***

Loading conditions and Boundary conditions applied on Target chamber are:

1. Convective heat transfer coefficient and Fluid temperature is applied in Radial channels.
2. Uniform volumetric heat generation is applied on window.
3. Convective heat transfer coefficient and Fluid temperature is applied in boiling region in Transient analysis and Uniform Heat flux is applied in case of Steady State analysis.
4. Convective heat transfer coefficient and Fluid temperature is applied on outermost curved part.
5. Symmetry Boundary conditions are applied on all the areas on XZ plane and YZ plane.

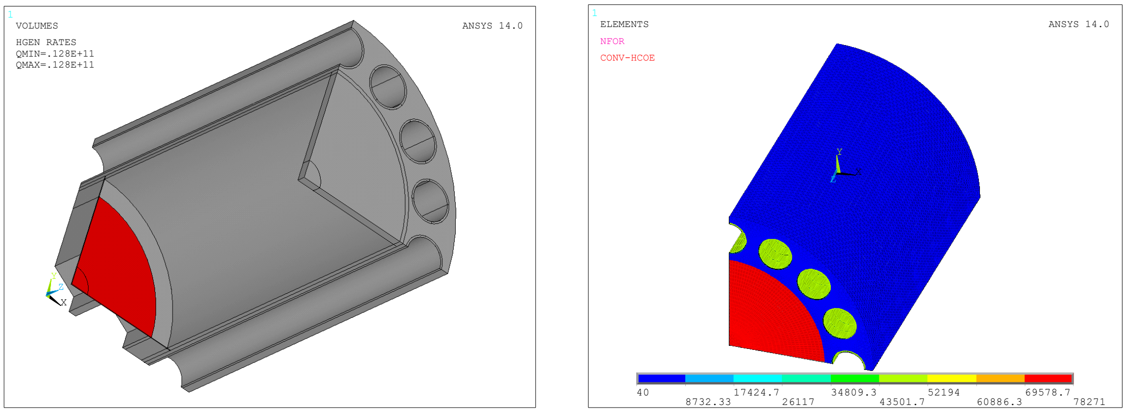


**Figure 21: Volumetric Heat Generation and Convective Heat Transfer Coefficient Boundary Conditions**

***For Structural Safety Analysis:***

Loading conditions applied on Target chamber are:

1. Uniform pressure on Target window from chamber liquid side.

2. Fixed support on window edges.

3. Symmetry Boundary conditions are applied on all the areas on XZ plane and YZ plane.

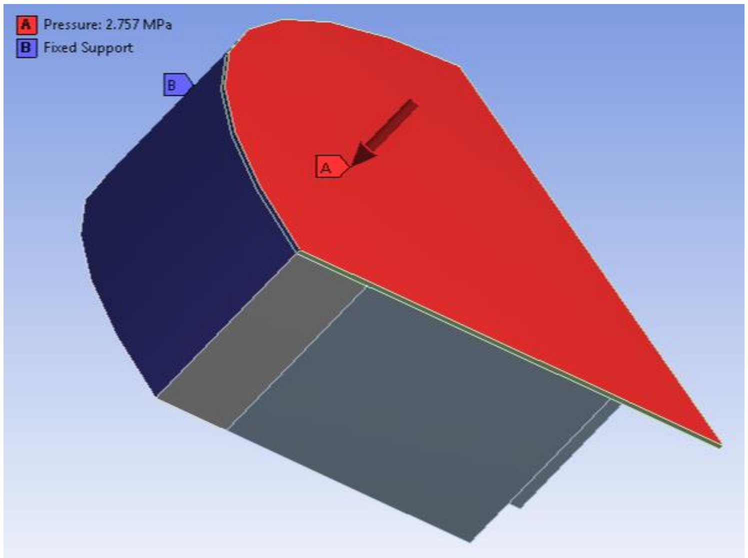


**Figure 22: Fixed support and constant Pressure Boundary Conditions**

## 6.5 Solution

Based on dimensions of target chamber, thermal conductivities, volumetric heat generation rate, heat transfer coefficient correlations and physics previously described, an ANSYS Parametric Design Language (ANSYS) code was written. ANSYS program, which uses finite element techniques to solve partial differential equations, was used to model the heat transfer. Symmetric boundary conditions were applied, so that the result obtained for $1/4^{th}$ part is valid for whole geometry. ANSYS steady state solution yielded wall temperatures variation, heat transfer rates in the radial direction and heat transfer rates in back plate direction. ANSYS transient analysis gives the void fraction with time. ANSYS structural analysis gives the region of maximum stress.

# CHAPTER 7

## RESULTS

The performance of Target chamber with different radial coolant channel dimension was examined. Steady state thermal analysis, Transient thermal analysis and Structural safety analysis were performed to analyze target chamber behavior under actual operation. The results obtained are compared.

***Steady State Thermal Analysis:***

Initially no external cooling was provided to the target chamber. Only ambient radiation heat transfer and natural convection boundary conditions were applied on the external surfaces during steady state thermal analysis. The result obtained is shown in Figure-23. It indicates that temperature in the target chamber is very high. To avoid this situation, another case was considered in which only the radial cooling channel heat transfer was introduced. The result is shown in Figure-24. This gives lower temperature of the target chamber compared to no external cooling case. But, the temperature was still found to be high. Finally, a third case was considered with both the radial channel and back jet cooling. The result is shown in Figure-25. It is evident from this result that both radial channel and back jet cooling will keep the temperature of target within a safe limit.

The heat transfer coefficient of radial channel ($h_r$) is nearly same for 0.5 mm and 1 mm radial channels. But, it is lower for 2 mm channel as shown in Table-1. This results into lower maximum temperature in target chamber with 0.5 mm and 1 mm channel as compared to 2 mm channel. The variation of temperature in target chamber with 0.5 mm, 1 mm and 2 mm radial channels is shown in Figure-25, 26 & 27. If we want to further decrease the maximum temperature than we can go for Helium cooling of window foil.

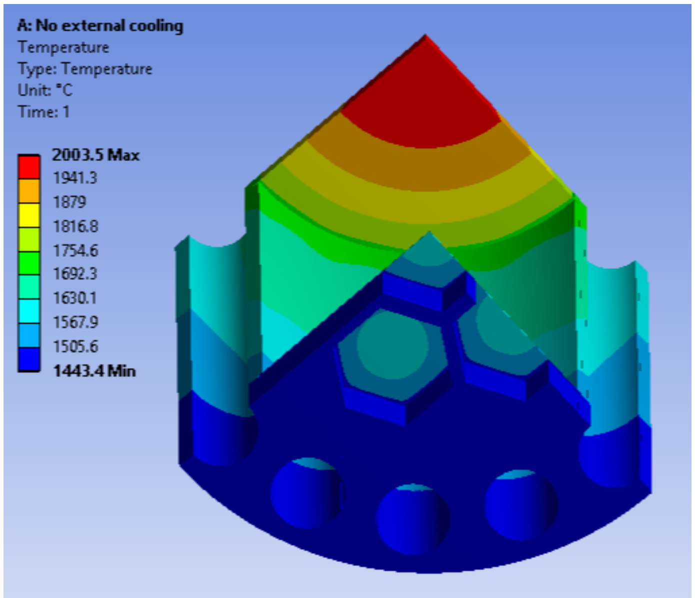


**Figure 23 :Temperature Variation in chamber under Steady State Thermal condition without any external cooling**

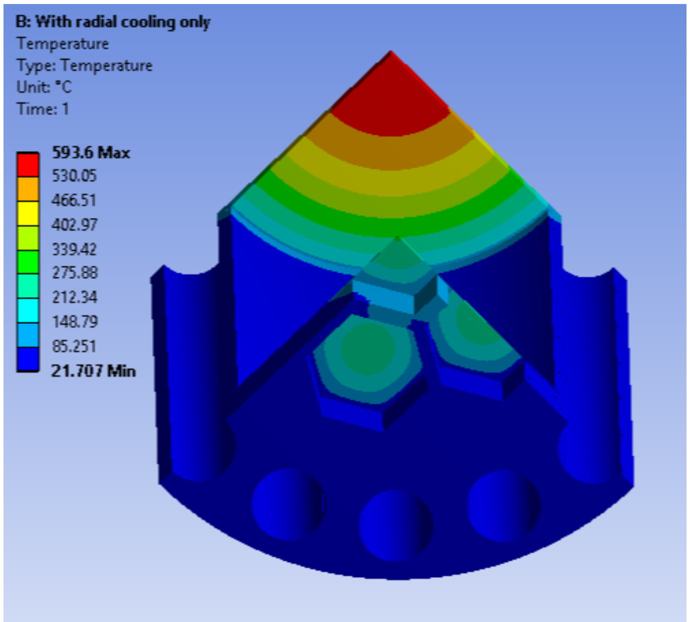


**Figure 24 :Temperature Variation in chamber under Steady State Thermal condition with only Radial cooling**

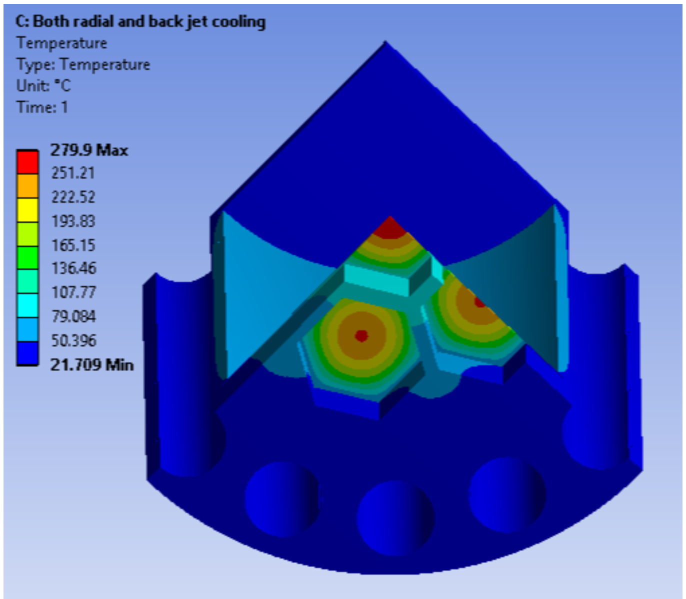


**Figure 25 :Temperature Variation in chamber under Steady State Thermal condition with Radial cooling and Back jet cooling of 2 mm channel**

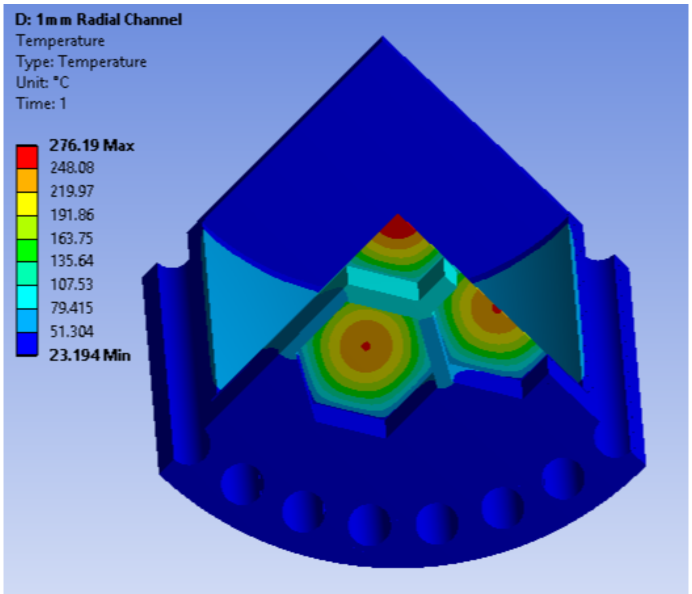


**Figure 26: Temperature Variation in chamber under Steady State Thermal condition with Radial cooling and Back jet cooling of 1 mm channel**

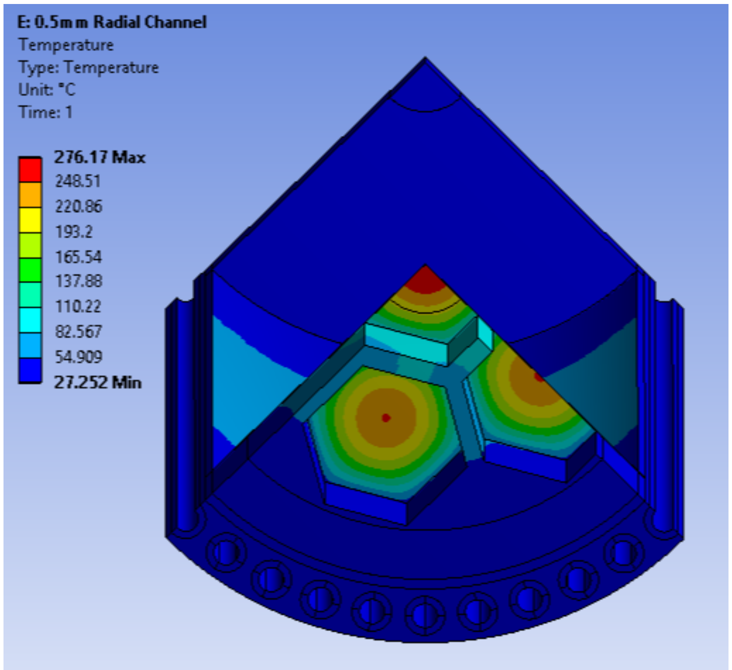


**Figure 27: Temperature Variation in chamber under Steady State Thermal condition with Radial cooling and Back jet cooling of 0.5 mm channel**

**Table 7: FEM(ANSYS) data for different radial channel diameter placed at 0.5 mm radially from Target chamber and cooled from both radial channel and back jet cooling**

| $d_r$(mm) | $n_T$ | $\dot{m}_r$(Kg/s) | $Q_{rad}$(W) | $T_{out,radial}$(°C) | $\dot{m}_b$(Kg/s) | $Q_{back}$(W) | $T_{out,back}$(°C) | $T_{max}$(°C) |
|---|---|---|---|---|---|---|---|---|
| 0.5 | 40 | 0.064 | 951.36 | 23.60 | 0.015 | 148.64 | 22.29 | 276.17 |
| 1 | 28 | 0.213 | 951.92 | 21.09 | | 148.08 | 22.28 | 276.19 |
| 2 | 16 | 0.505 | 948.48 | 20.45 | | 151.52 | 22.33 | 279.9 |

To calculate the $T_{out,radial}$ and $T_{out,back}$ , an energy balance equation can be written as

$$Q_{net} = \dot{m} c_f (T_{out} - T_{in})$$

$Q_{net}$ - Heat output to radial or back jet ṁ - Mass flow rate of coolant in manifold

$T_{out}$ and $T_{in}$ - Temperature of coolant at outlet manifold and inlet manifold

$T_{out}$ observed in both radial and back jet is not very large than $T_{in}$ because of high value of specific heat capacity of liquid and its mass flow rate.

Note that maximum temperature ($T_{max}$) is occurring on Havar foil centre.

***Transient Thermal Analysis:***

Transient thermal analysis was done to observe the behavior of target chamber during initial phase of operation. The variation of Void fraction with time for FEM(ANSYS) and Lumped System model was compared. The results obtained was plotted. The variation in FEM(ANSYS) and Lumped system model is due to assumptions of no heat transfer between Window and Target liquid.

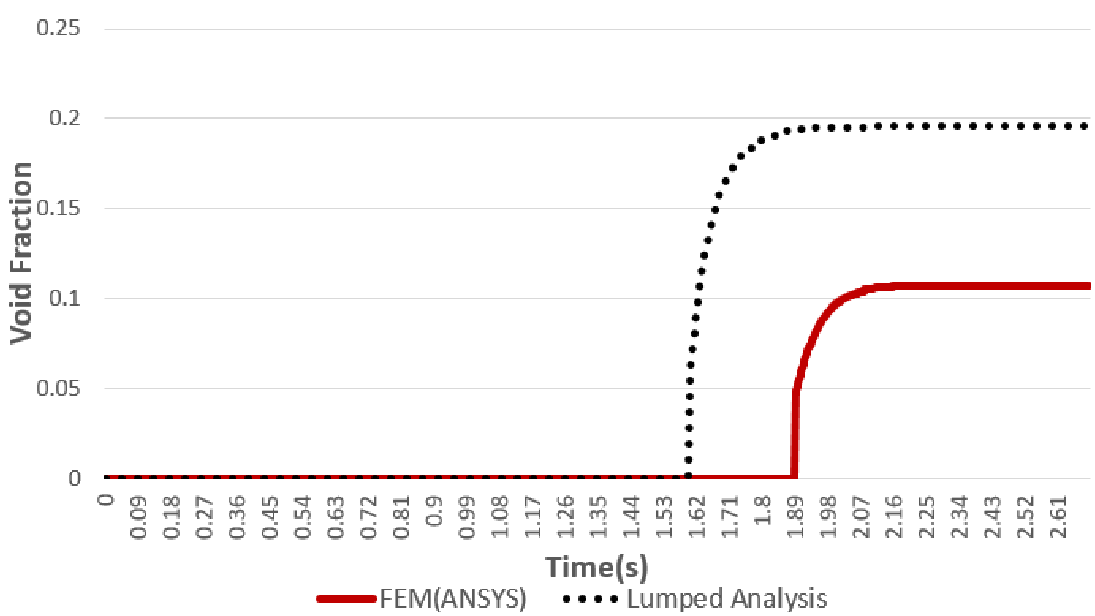


**Figure 28: Void Fraction variation with time comparison in Transient analysis between FEM (ANSYS) and Lumped Analysis**

***Structural Safety Analysis:***

Due to very thin size of Window under high pressure of 400 psia (2.75 MPa) Target liquid, it is more prone to rupture than other part of Target chamber. Structural safety analysis was done to investigate the maximum stress region in Havar Window under operating condition. The result of stress variation in different region of Window is shown in figure below. The maximum stress obtained is 1539.8 MPa which is lower than Yield Strength of HAVAR foil with Cold Rolled (85 %) and Cold Rolled & Heat Treated shown in Table 6. The factor of safety for Cold Rolled & Heat Treated is 1.34, which is highest among the materials given in Table-6.

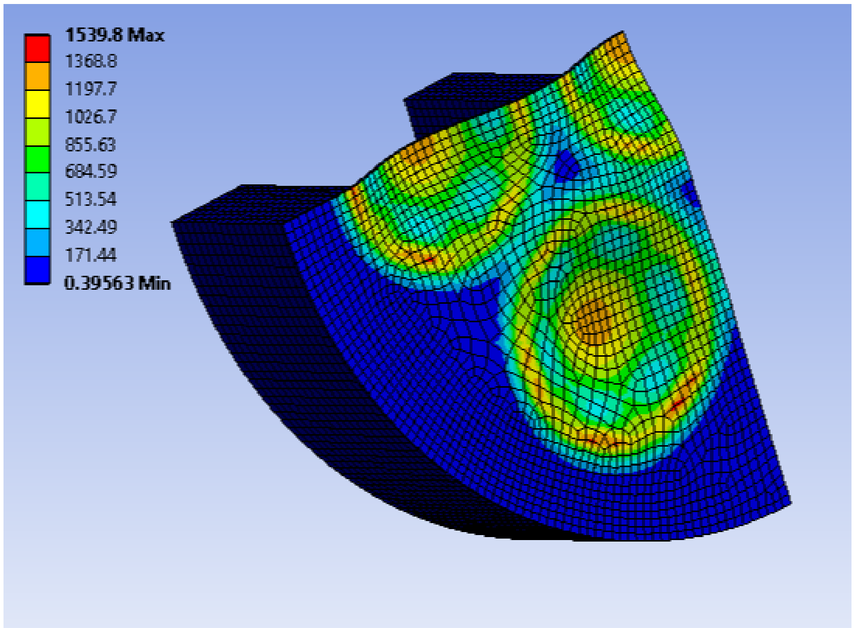


**Figure 29: Von Mises Stress(MPa) in HAVAR foil due to 400 psia (2.75 MPa) pressure**

# CHAPTER 8

## CONCLUSIONS

### 8.1 Summary and Conclusions

The aim of this project was the thermal analysis design of Thermosyphon water targets for production of $^{18}F$ radioisotope for use in PET medical imaging. The designed target accommodates the highest heat input of 1100 W with the minimum liquid volume without surpassing thermal limits.

An OCTAVE code which was written for lumped heat analysis showed that after some transients, a steady state will be achieved. This result was verified by FEM(ANSYS) model. Difference in predicted void fraction and chamber wall temperature was observed between OCTAVE and ANSYS result. This difference can arise due to assumptions taken during modeling.

Table-1 shows that for a given pressure difference across inlet and outlet manifold, 1 mm diameter channel has advantage over other radial channel dimensions. It also has lower maximum temperature than 2 mm channel and $V < 2$ m/s that will prevent Flow Induced Vibration in pipe. Moreover, it easy to manufacture 1 mm channel as compared to 0.5 mm channel.

Steady state thermal analysis data obtained from FEM(ANSYS) shows that for radial channels of different dimensions placed at 0.5 mm away radially from target chamber have nearly 86% of heat rejected to radial cooling channel and 14% to back jet cooling. So, it is evident that radial coolant channels are more effective in extracting heat from target chamber. Moreover, the temperature difference between inlet and outlet manifolds of cooling water is very low due to high mass flow rate and high specific heat capacity of water.

Critical heat flux calculation shows that for a target pressure of 400 psia (2.75MPa), we cannot increase current beyond 50 μA. As $R_{pta}^{crit}$ will come down which leads to high $q''_{avg}$ and hence high temperature of Window surface.

Theoretical stress analysis shows that for given Window thickness, applied pressure and Boundary condition, maximum stress decreases with decreasing diameter of Window. Moreover, FEM(ANSYS) structural stress analysis shows that for a large diameter Window of HAVAR and Honeycomb support structure of Aluminum, the stresses are within yield limit.

A 3D model shown in Figure-1 was created in SOLIDWORKS which shows different parts of PET Target.

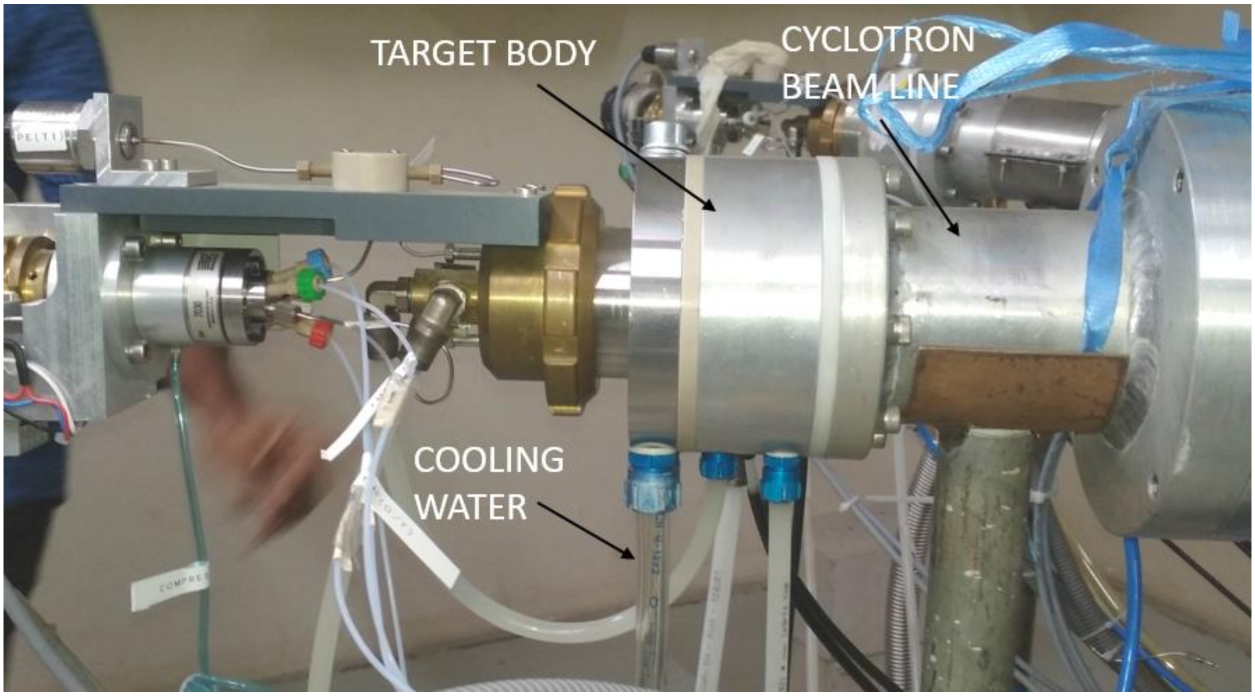


**Figure 30: MCP PET Target located in Chakgaria Campus of VECC**

Schematic of PET Target installed in VECC campus is shown in Figure-30. A similar type of Target is to be constructed based on the present study and will be rigorously tested in this facility.

## 8.2 Future Work

A detailed investigation using CFD (Computational Fluid Dynamics) is needed to be carried out to simulate the two phase fluid flow and heat transfer inside the target chamber. An Experimental testing will be done using a fabricated model and compare the results with the FEM code results developed in this study.

# REFERENCES


1. ANSYS, version 14.0
2. Berridge MS, Voelker KW, and Bennington B. "High-yield, low-pressure [$^{18}$O] water targets of titanium and niobium for $F^{18}$ production on MC-17 cyclotrons," Applied Radiation and Isotopes, vol. 57, 2002.
3. Bergman TL, Lavine AS, Incropera FP and Dewitt DP. Fundamentals of Heat and Mass Transfer, 7$^{th}$ edition, John Wiley & Sons, 2011.
4. Berridge MS and Kjellström R. "Design and use of silver [$^{18}$O] water targets for [$^{18}$F] fluoride production," Applied Radiation and Isotopes, vol. 50, 1999.
5. Çengel YA and Ghajar AJ. Heat and Mass Transfer: Fundamentals & Applications, 5$^{th}$ edition, McGraw-Hill Publication, 2015.
6. Clark JC. "High-Powered Cyclotron Recirculating Targets for Production of the $^{18}$F Radionuclide," Master of Science Thesis. North Carolina State University, 2004.
7. Engineering ToolBox, (2003). Maximum Flow Velocities in Water Systems. Available at: https://www.engineeringtoolbox.com/flow-velocity-water-pipes-d_385.html [15.11.2020].
8. Faw RE and Shultis JK. Radiological Assessment: Sources and Doses. Illinois: American Nuclear Society, 1999.
9. Ghiaasiaan SM. Two-Phase Flow, Boiling and Condensation in Conventional and Miniature Systems, 1$^{st}$ edition, Cambridge University Press, 2008.
10. Helus F and Ruth TJ. Proceedings of the first workshop on Targetry and Targetry chemistry. DKFZ Press Department, Canada, 1987, pp 5-40.
11. Hess E, Takàcs S, Scholten B, Tàrkànyi F, Coenen HH, and Qaim SM. "Excitation function of the $^{18}$O(p,n)$^{18}$F nuclear reaction from threshold up to 30 MeV," Radiochimica Acta, vol. 89, issue 6, 2001, pp 357.
12. Idelchick IE. Handbook of Hydraulic Resistance, 3$^{rd}$ edition, Jaico Publishing House, 2008.
13. Lienhard JP and Dhir VK. "Hydrodynamic Prediction of Peak Pool-boiling Heat Fluxes from Finite Bodies," *ASME Journal of Heat Transfer*, vol. 95, 1973.
14. Martin H. "Heat and Mass Transfer Between Impinging Gas Jets and Solid Surfaces," Advances in Heat Transfer, vol. 13, 1977.

15. Metals HP. HAVAR – "TECHNICAL DATA SHEET. Hamilton Precision Metals, 1991.
16. Nuclides and Isotopes. 15th Edition. California: General Electric and KAPL, 1996.
17. OCTAVE, version 5.1.0
18. Ollinger JM and Fessler JA. “Positron Emission Tomography,” IEEE Signal Processing Magazine, vol. 14, 1997, pp 43-44.
19. Phelps ME. PET: Molecular Imaging and Its Biological Applications. New York: Springer, 2004.
20. Peeples JL. “Design and Optimization of Thermosyphon Batch Targets for Production of $^{18}F$,” Master of Science Thesis. North Carolina State University, 2006.
21. Peeples JL. “Design and Testing of Thermosyphon Batch Targets for Production of $^{18}F$,” Doctor of Philosophy Thesis. North Carolina State University, 2008.
22. Roberts AD, Daniel LC and Nickles RJ. “A high power target for production of [$^{18}F$] fluoride,” Nuclear Instruments and Methods in Physics Research B, vol. 95, 1995.
23. Roberts AN. “Thermosyphon Targets Designed for the Production of $^{18}F$ for Use in Positron Emission Tomography,” Master of Science Thesis. North Carolina State University, 2002.
24. Satyamurthy N, Amarasekera B, Alvord CW, Barrio JR and Phelps ME. Tantalum [$^{18}O$] water target for the production of [$^{18}F$] fluoride with high reactivity for the preparation of 2-deoxy-2-[$^{18}F$] fluoroD-glucose, Molecular Imaging & Biology, vol. 4, issue 1, 2002, pp 65-70.
25. Timoshenko SP and Krieger SW. Theory of Plates and Shells, 2nd edition, McGraw-Hill Publication, 2010.
26. SOLIDWORKS, version 2019
27. Stokely MH. “Deployment, Testing and Analysis of Advanced Thermosyphon Target Systems for Production of Aqueous [$^{18}F$] Fluoride via $^{18}O(p,n)^{18}F$,” Doctor of Philosophy Dissertation. North Carolina State University, 2008.
28. Stokely MH. “Advanced Thermosyphon Targets for Production of the $^{18}F$ Radionuclide,” Master of Science Thesis. North Carolina State University, 2007.
29. Valk PE, Bailey DL, Townsend DW and Maisey MN. Positron Emission Tomography: Basic Science and Clinical Practice. New York: Springer-Verlag, 2003.

30. Wen D and Ding Y. "Natural Convective Heat Transfer of Suspensions of Titanium Dioxide Nanoparticles (Nanofluids)," IEEE Transactions on Nanotechnology, vol. 5, no. 3, 2006.
31. Wieland B, Illan C, Doster JM, Roberts A, Runkle R, Rowland C and Bida J. "Self-Regulating Thermosyphon Water Target for Production of F-18 Fluoride at Proton Beam Power of 1 kW and Beyond," Proceedings of the Ninth International Workshop on Targetry and Target Chemistry. Turku, Finland: 2002.
32. Zeisler SK, Becker DW, Pavan RA, Moschel R and Rühle H. "A water-cooled spherical niobium target for the production of $^{18}F$," Applied Radiation and Isotopes, vol. 53, 2000.